Table 5.2 Statistical values for results of cube tests

| Series | Total No. of cubes | Cube strength | | Density | |
|---|---|---|---|---|---|
| | | Mean (MPa) | Coefft. of variation (%) | Mean ($kg/m^3$) | Coefft. of variation (%) |
| F1 | 22 | 34,16 | 13,56% | 2416 | 1,01% |
| F2 | 25 | 40,30 | 7,84% | 2471 | 1,45% |
| F3 | 36 | 30,90 | 2,89% | 2440 | 0,78% |

All series had cement/water ratio of 1,83, for which the mean target strength was 37MPa with a minimum design strength of 28MPa[83]. Thus, results for series F1 were about 10 per cent below target, series F2 results were 6 per cent higher than target, and series F3 results were 16 per cent below target strength. In terms of standard deviations, the values for the present tests are below the figure of 5MPa which is given in SABS 0100[84] as being an appropriate figure for good site control. It seems that any lack of control of curing temperatures for series F1 and F2 has not impaired the overall results seriously. The very similar mean values and low C.V.s for concrete densities indicate that uniform compaction was achieved and that the difference in densities could not account for the difference in mean cube strengths.

With reference to series F2, the cubes and associated fracture beams F2/13 to 15 and 24 to 26 were cured in a water bath at a controlled temperature (20°C), and achieved a mean cube strength 2,2 per cent higher than the overall mean for series F2. This indicates that very similar curing temperatures were achieved for the specimens cured on the laboratory floor and those in the curing tank, and that the floor specimens were maintained in a saturated state during curing. The fracture beams F2/4, 11 to 15, 22 to 26 and associated cubes used crushed granite stone in place of crushed quartzite stone (see appendix A). The use of this coarse aggregate has not materially affected the cube strengths of the concrete.

The significantly lower cube strengths for series F3 require some explanation. The excellent consistency between batches cast on any one day, and between batches cast on different days (table 5.1) indicates that very good quality control was achieved. Two possible reasons for the lower strengths present themselves:- the first is that the batch of cement used for this series was significantly different from the cement used two and a half years previously for the earlier series, but whether this difference originated in the factory or during transport and storage is not clear; the second is that very much higher slumps were observed for series F3 which may in some way have affected the strength. (See appendix A for slump details). Clearly, the properties of the aggregates for series F3 were different from those for series F1 and F2 from a slump point of view, since identical proportions of solids were used for all series. Considering that high slumps tend to cause bleeding, particularly for the rather coarse crusher sands used in the present tests, it is possible that water was trapped under aggregate particles before initial set, causing bleed voids or flaws exhibiting lower interface bond strengths. Since cubes are tested with the load axis at right angles to the direction of casting, these potential voids or zones of low bond strength would be orientated such as to enhance failure by vertical cracking. Inspection of fractured cubes and fractured faces of the beams did not, however, reveal macro-voids. A positive conclusion for the lower cube strengths is not easy to arrive at but the point is discussed in more detail in appendix C.

## 5.2.2 MODULUS OF RUPTURE

### SERIES F1

The MR tests used third-point loading and a span/depth ratio of six. Previous tests[60] showed that somewhat lower values of MR are obtained using the longer beams. Without modifying the results for the effects of span/depth ratio or cube/cylinder tests, they were consistent with the results of Walker and Bloem[85] shown in figure 5.3. The main disadvantage of the present results was that they were based on a single specimen per batch, and hence their usefulness was obviously limited. Nevertheless, as control tests on flexural strength they have shown that the various batches conformed to expected trends.

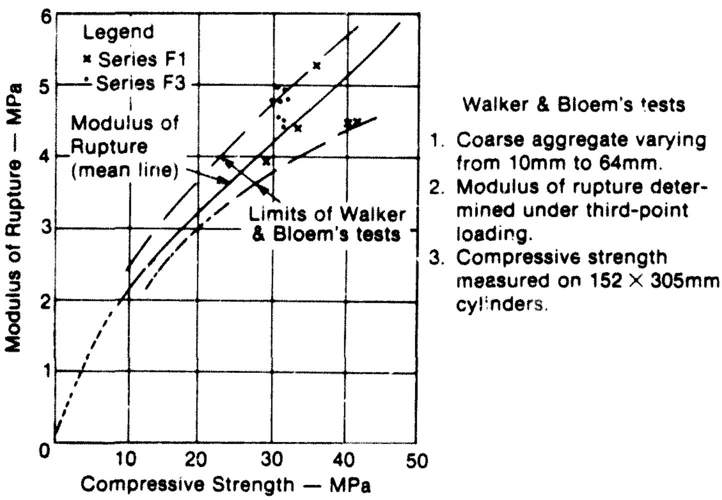


Figure 5.3 Results of modulus of rupture tests compared with those of Walker and Bloem[85]

### SERIES F3

MR tests for this series were conducted as control tests and to assess notch-sensitivity by providing a basis against which to compare results of the notched MR beams (see 5.4 later). The tests used a span/depth ratio of four and centre-point loading, in order to be consistent with the loading of the fracture beams. The results are plotted without modification in figure 5.3 as a direct comparison with results from Walker and Bloem's tests[15] and from series F1 tests. Despite the lower mean cube strengths of series F3, the MR results generally plotted higher than those for series F1, due to the smaller span/depth ratio and the use of centre-point loading. Nevertheless, the results appeared consistent, and a fairly low coefficient of variation of 8,2 per cent was obtained.

### 5.2.3 MODULUS OF ELASTICITY

#### SERIES F1 AND F2

Elastic modulus values for the concretes were required for use in the fracture calculations. These values were measured on beams for series F1 and on prisms for series F2. Previous work by the author[86] indicated that there was a difference between results from beam and prism tests. Hence the prism results have been modified to represent equivalent beam results, firstly for comparison between the two series, and secondly since the fracture tests used beam specimens and the flexural E is probably more appropriate to the fracture calculations. In ref. 86 it was noted that a good deal more work would be required to characterise more fully the effect of, say, differing span/depth ratios on flexural E. For the present tests, however, the relationship between flexural E and prism E quoted in ref. 86 was used, viz.

$$\text{flexural E/prism E} = 1{,}055 \qquad (5.4)$$

Table 5.3 shows the measured values of mean cube strength $\bar{f}_{cu}$ and elastic modulus E for particular batches. The elastic modulus is expressed as an equivalent flexural E using the ratio given in equation (5.4). Only one value of elastic modulus was measured for the batches of series F1, and only two values for the batches of series F2. Therefore a better estimate of elastic modulus was obtained by using an averaging technique to obtain a mean value of an appropriate parameter for the given series, and then this mean value was used to infer an E value for the particular batches. In this way, the limited measurements of E values for each batch could be overcome, and E values could be inferred for those batches where they were not measured.

There are a number of accepted empirical relationships between elastic modulus and compressive strength[87]. The appropriate parameter chosen in this case was $E/\sqrt{f_{cu}}$. (It might be noted that the use of a square-root term in the above expression is followed by the ACI[88], by Davis[89], and by the CEB/FIP(1970)[90]. The later model code of the CEB/FIP(1978)[91] uses an exponent of 1/3 rather than 1/2). The adoption of this parameter allowed the effect of cube strength, a mean value of which was confidently obtained in the present tests, to be included in the determination of the elastic modulus.

The results of the averaging technique to obtain better overall E values are shown in table 5.3. The mean value of $E/\sqrt{f_{cu}}$ for each series was used together with the mean strengths for each particular batch to obtain the required E value. The values in the third and fourth column of table 5.3 have been plotted in figure 5.4 as a comparison with Davis's results[89]. Bearing in mind that flexural E values are of the order of 12 per cent higher[86] than cylinder E values which Davis used, it can be seen that the present results accord well with results for other South African concretes.

## SERIES F3

The prism E values are given in table 5.1(c). Three specimens were tested for any particular batch of fracture beams, and reasonable consistency was obtained between the mean values of batches on

Table 5.3 Use of an averaging technique to obtain values of elastic modulus for fracture calculations (series F1 and F2)

| Series | Specimen numbers | Mean cube strength ($\bar{f}_{cu}$) (MPa) | Measured elastic modulus (E) (equivalent flexural value) (GPa) | | Ratio $E/(\bar{f}_{cu})^{\frac{1}{2}}$ | Elastic modulus from $\bar{f}_{cu}$ and mean value of $E/(\bar{f}_{cu})^{\frac{1}{2}}$ (GPa) |
|---|---|---|---|---|---|---|
| F1 | F1/1<br>2 | 40,01 | 33,42 | Quartzite Course Aggregate | 5,28 | 34,66 |
| | 3<br>4 | 40,75 | 33,27 | | 5,21 | 34,98 |
| | 5<br>6 | 32,61 | 36,00 | | 6,30 | 31,29 |
| | 7<br>8 | 28,69 | 32,09 | | 5,99 $\bar{x}$ = 5,48 | 29,35 |
| | 9<br>10<br>11 | 35,34 | - | | - | 32,58 |
| | 12<br>13<br>14 | 69,85 | 38,78 | | 4,64 | 32,03<br>($\bar{f}_{cu}$=34,16) |
| F2 | F2/1.5,6,<br>16,17 | 40,40 | 31,95 | | 5,03 | 33,24 |
| | 2,7,8,<br>18,19 | 35,82 | 33,83 | | 5,65 | 31,30 |
| | 3,9,10,<br>20,21 | 43,54 | - | | - $\bar{x}$ = 5,23 | 34,51 |
| | 4,11,12,<br>22,23 | 40,92 | 33,20 | Granite Coarse Agg. | 5,19 | 33,46 |
| | 13,14,15,<br>24,25,26 | 41,17 | 32,43 | | 5,05 | 33,56 |

**Note** $\bar{x}$ in each case refers to the mean of the set of results different days. This was not always true within batches produced on one particular day. Table 5.1(c) shows that quite large variations occurred for certain sets of fracture beams. A statistical test (the "T" test)[82], the object of which is to determine whether a particular result can be regarded as an outlier and therefore discarded, was applied to the extremes of the results in table 5.1(c), all the results being taken together. The test showed that all results could be regarded as valid and none were discarded. However, the mean values for the different sets of results accorded well, except only for the value associated with beams F3/24 to 26. The same "T" test was applied to this value, with all the means being taken together; in this case the test showed that this value could be regarded as an outlier, and could be retained on its own. The ratio of flexural E to prism E of 1,055, explained before, was applied to the prism values, and the results compared with Davis's[89] curve in figure 5.4. It can be seen that generally the values fall on the low side, but within the limits of Davis's results. The values are substantially below the values for series F1 and F2, notwithstanding the slightly lower mean cube strengths of series F3.

In chapter 6 the elastic modulus values are required to calculate beam compliances. It was found that using the low values measured on the prisms of series F3 led to consistently low values of initial compliance when compared with theoretical values for the various notch depths. This was in sharp contrast to the results for series F1 and F2, where mean values of initial compliance accorded very well with theory. It was thus suspected that the low E values obtained from the prisms were not really representative of the flexural E values being exhibited by the fracture beams of series F3. An explanation had therefore to be sought which would account for the E values of series F1 and F2 falling generally above Davis's mean line and the prism results for series F3 falling generally below the same line.

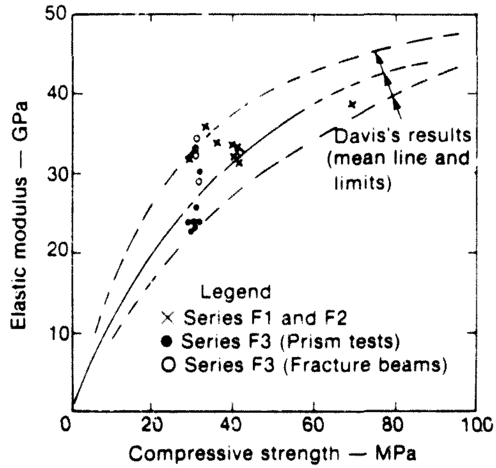


Figure 5.4 Results of elastic modulus tests compared with those of Davis for South African concretes[89]

The most likely reason for the above-mentioned anomaly and for the variation in individual elastic modulus values is the effect of slump on measured modulus. Thompson and Davis[93] have shown that static elastic modulus may vary very significantly depending on the slump at which the concrete was cast, higher slumps giving lower elastic moduli. Their results have been reworked to provide a relationship between the ratios of the 28 day elastic moduli of concrete cast at a particular slump and concrete with a slump of 100mm, versus the "as-cast" slump values. This relationship is shown in figure 5.5 where a clear trend is evident. The results for series F3 have similarly been reworked and also plotted in figure 5.5.

The scatter for the present results was greater than that of Thompson and Davis, but a trend is nevertheless evident. This trend is much steeper than the other curve, indicating that modulus was very sensitive to slump. It is also significant that the higher modulus values for beams F3/24 to 26 corresponded with the lowest slump for any of the batches (i.e. a mean slump of 87mm).

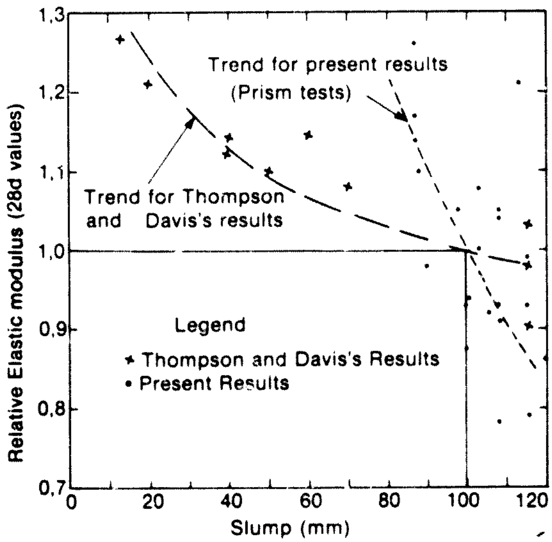


Figure 5.5 Effect of "as-cast" slump on static elastic modulus of concrete; results from Thompson and Davis[11] and series F3

Since the only substantial difference between the plastic state of the concretes of series F1/F2 and series F3 was the higher slump for series F3, it is proposed that this factor has caused the unacceptably low prism E values of the latter series. Appendix C contains a supporting argument for this.

In view of the above, elastic modulus values for series F3 were obtained directly from the results of the fracture beams themselves. The technique involved assessing initial compliances of the notched beams and inferring E values using the theoretical relationships between E, unnotched compliance, and notched compliance. Details are given later in 6.5. It was felt that such a technique was entirely justified since the results of series F1/F2 had shown that E values measured on medium to low slump concretes gave initial compliances which agreed well with theoretical values.

The inferred E values for series F3 are given in table 5.4, and it can be seen that individual beam values have been averaged for the different beam sizes. The values in table 5.4 accord remarkably well with the values for series F1 and F2, which should be expected in view of the similar materials used in all series. Finally, the inferred E values for series F3 have been plotted in figure 5.4, where it can be seen that they lie above Davis's mean line which is consistent with the results for series F1 and F2. (It should be noted that the larger variable section beams gave a mean E value about 10 per cent higher than the value for the smaller constant section beams, but that the coefficients of variation of the results for E were very low at 6,1 per cent and 8,3 per cent respectively).

Table 5.4 Values of elastic modulus from fracture beams (series F3)

| Specimen numbers | Beam depth (mm) | Mean E for given beam depth (GPa) |
|---|---|---|
| F3/1-4 | 500 | 34,29 |
| F3/5-12 | 300 | 33,68 |
| F3/13-16 | 200 | 32,50 |
| F3/17-20 24-26,28 | 100 | 28,95 |

Note

1. Results for beams 2 -23,29 have been omitted since these beams had sawn notches.

2. Result for beam 27(40,03 GPa) was an outlier.

### 5.2.4 CONCLUSIONS, MATERIALS CONTROL TESTS

1. The materials tests were conducted primarily as controls on material quality (i.e. batching, mixing, compaction and curing). The number of tests was therefore limited.

2. Significant variations in compressive strength occurred between the cubes of the three series. In the case of series F1 and F2, for which single batches of cement and aggregates were used, the variations were probably attributable to differences in mean curing temperatures. For series F3 where completely different batches of cement and aggregates were used, possible reasons for the lower strengths were different cement quality and the higher slumps experienced by these mixes.

3. The only parameter required from the materials tests for use in the fracture calculations was the modulus of elasticity. For series F1 and F2 the individual E results were processed by means of an averaging technique employing the parameter $E\sqrt{\bar{f}_{cu}}$ which included the mean value of the individual batches of cube results ($\bar{f}_{cu}$). This allowed the disadvantage of the limited number of E values to be overcome, and produced E values for the individual beams that could be used with greater confidence.

4. For series F3, the E results obtained from prism tests were considered to be unrepresentative of the stiffnesses of the fracture beams themselves, due to the influence of bleeding. Consequently, E values were inferred from the fracture records, and these values accorded well with the values for series F1 and F2. For series F1 and F2, prism E values were converted to equivalent flexural values for use in the fracture calculations. This was not considered necessary for series F3 since the E values were inferred from the fracture records.

5. Examination of the statistical coefficients of variation and comparison of the results with expected values for cube

strengths, MR, and E showed that the results were generally consistent with other quoted work.

## 5.3 BASIC DATA FROM FRACTURE TESTS.

The fracture tests were conducted on crack-notched bend specimens due to the relative simplicity of this type of test. Other techniques of fracture testing are the use of compact tension specimens, double cantilever beams, direct tension specimens, and double torsion specimens. The intention was to test very large fracture specimens, and the beam test was suitable for the present work. The output from the tests included mid-span load and deflection, and for series F3 also ultrasonic pulse transit times and strains across the notched section; this primary output was processed to produce fracture parameters and information concerning the fracture process.

A summary of the basic fracture test data is given in table 5.5, in the form of:-

$F_{max}$(KN) - maximum machine load recorded during the test
$\delta_{Fmax}$(mm) - mid-span beam deflection corresponding to $F_{max}$
$\delta_m$(mm) - deflection when machine load dropped to zero
$\delta_u$(mm) - deflection at ultimate failure
$A_{F,\delta}$(Nm) - area under the load-deflection curve

The load-deflection records of nineteen typical beams which cover the full range of beam types are presented in tabular form in appendix D. These beams were considered representative of the various types and shapes, and were used for detailed analysis of fracture behaviour. Data from other beams was also frequently used to get a full spread of results where necessary. (Experimental data of all the beams is available if required).

Table 5.5 Basic data from fracture tests

(a) Series F1

| Specimen identification | $F_{max}$ (kN) | $\delta_{F\,max}$ (mm) | $\delta_m$ (mm) | $\delta_u$ (mm) | $A_{F,\delta}$ (Nm) |
|---|---|---|---|---|---|
| F1/1(500/0,2) | (19,45) | (0,145) | - | No data available due to inability of strip-chart recorder to accurately record $\delta_u$ | - |
| 2(500/0,2) | 16,78 | 0,126 | 1,203 | | 5,335 |
| 3(500/0,4) | 9,34 | 0,152 | 1,186 | | 4,106 |
| 4(500/0,4) | 10,88 | 0,195 | 1,509 | | 6,028 |
| 5(300/0,2) | 14,27 | 0,134 | - | | - |
| 6(300/0,2) | 14,88 | 0,136 | 1,465 | | 4,969 |
| 7(200/0,4) | 4,30 | 0,069 | 2,029 | | 2,046 |
| 8(200/0,4) | 4,04 | 0,102 | 1,934 | | 1,67[illegible] |
| 9(100/0,25) | 4,31 | 0,050 | 2,104 | | 1,327 |
| 10(100/0,25) | 4,23 | 0,044 | 1,991 | | 1,005 |
| 11(100/0,25) | 5,62 | 0,079 | 2,380 | | 1,777 |
| 12(100/0,4) | 4,57 | 0,077 | 1,836 | | 1,444 |
| 13(100/0,4) | 2,90 | 0,049 | 1,722 | | 0,894 |
| 14(100/0,4) | 4,31 | 0,068 | 1,398 | | 0,913 |

Table 5.5 (Continued)

(b) Series F2

| Specimen identification | $F_{max}$ (kN) | $\delta_{F\,max}$ (mm) | $\delta_m$ (mm) | $\delta_u$ (mm) | $A_{F,\delta}$ (Nm) |
|---|---|---|---|---|---|
| F2/1(800/0,2) | 28,12 | 0,398 | - | | - |
| 2(800/0,4) | 10,49 | 0,185 | 0,359 | No data available due to inability of strip-chart recorder to accurately record $\delta_u$ | 1,652 |
| 3(800/0,4) | 13,06 | 0,235 | 0,558 | | 2,708 |
| 4(800/0,4) | 12,68 | 0,265 | 0,325 | | 2,218 |
| 5(100/0,25) | (5,03) | (0,049) | (1,289) | | (0,803) |
| 6(100/0,25) | 5,07 | 0,055 | 1,241 | | 1,137 |
| 7(100/0,25) | 5,38 | 0,060 | 1,804 | | 1,325 |
| 8(100/0,25) | 5,59 | 0,075 | 1,825 | | 1,481 |
| 9(100/0,4) | 3,53 | 0,067 | 1,213 | | 0,737 |
| 10(100/0,4) | 3,39 | 0,062 | 1,509 | | 0,913 |
| 11(100/0,4) | 2,98 | 0,060 | 1,184 | | 0,654 |
| 12(100/0,4) | 4,30 | 0,074 | 1,747 | | 1,200 |
| 13(100/0,4) | 3,57 | 0,072 | 1,919 | | 1,109 |
| 14(100/0,4) | 3,10 | 0,053 | 2,654 | | 1,051 |
| 15(100/0,4) | 3,13 | 0,066 | 1,719 | | 0,826 |
| 16(100/0,5) | 0,87 | 0,095 to 0,138 | 1,833 | | 0,502 |
| 17(100/0,5) | 0,72 | 0,020 to 0,040 | 1,108 | | 0,188 |
| 18(100/0,5) | 0,78 | 0,085 | 0,963 | | 0,229 |
| 19(100/0,5) | 0,92 | 0,094 | 1,742 | | 0,494 |
| 20(100/0,5) | 0,92 | 0,080 | 0,573 | | 0,205 |
| 21(100/0,5) | 1,00 | 0,095 to 0,116 | 1,079 | | 0,329 |

Table 5.5 (Continued)

(b) Series F2 (Continued)

| Specimen identification | $F_{max}$ (kN) | $\delta_{max}$ (mm) | $\delta_m$ (mm) | $\delta_u$ (mm) | $A_{F,\delta}$ (Nm) |
|---|---|---|---|---|---|
| F2/22(100/0,5) | 1,04 | 0,126 | 1,050 | See note below* | 0,387 |
| 23(100/0,5) | 0,92 | 0,086 | 0,945 | | 0,269 |
| 24(100/0,5) | 0,92 | 0,115 | 1,957 | | 0,555 |
| 25(100/0,5) | 0,90 | 0,160 | 1,556 | | 0,410 |
| 26(100/0,5) | 1,00 | 0,158 | 1,910 | | 0,549 |

* No data available due to inability of strip-chart recorder to accurately record $\delta_u$

Table 5.5 (Continued)

(c) Series F3

| Specimen identification | $F_{max}$ (kN) | $\delta_{Fmax}$ (mm) | $\delta_m$ (mm) | $\delta_u$ (mm) | $A_{F,\delta}$ (Nm) |
|---|---|---|---|---|---|
| F3/1(500/0,2) | 16,00 | 0,238 | 1,253 | 1,754 | 7,011 |
| 2(500/0,2) | 18,74 | 0,308 | 1,297 | 2,506 | 7,193 |
| 3(500/0,4) | 8,70 | 0,219 | 0,902 | 1,504 | (2,821) |
| 4(500/0,4) | 9,03 | 0,251 | 1,403 | 2,945 | 3,638 |
| 5(300/0,2) | 10,35 | 0,183 | 1,795 | - | 4,446 |
| 6(300/[illegible]) | 10,15 | 0,164 | 2,381 | 4,5[illegible] | 4,147 |
| 7(300/0,25) | 9,025 | 0,168 | (2,530) | - | 4,448 |
| 8(300/0,25) | 9,025 | 0,187 | 2,722 | 3,822 | 4,490 |
| 9(300/0,25) | 10,60 | 0,228 | 3,133 | 5,119 | 6,163 |
| 10(300/0,4) | 6,83 | 0,162 | 2,017 | 2,506 | 3,504 |
| 11(300/0,4) | 5,71 | 0,148 | 2,763 | 3,759 | 2,337 |
| 12(300/0,4) | 5,60 | 0,140 | 2,443 | 3,822 | 2,456 |
| 13(200/0,2) | 9,45 | 0,096 | 3,252 | 4,010 | 3,759 |
| 14(200/0,2) | 8,95 | 0,096 | 2,512 | 3,759 | 3,449 |
| 15(200/0,4) | 4,84 | 0,102 | 2,318 | 3,527 | 2,575 |
| 16(200/0,4) | 5,41 | 0,094 | 2,851 | 4,010 | 3,225 |
| 17(100/0,2) | 5,45 | 0,059 | 3,596 | 5,012 | 2,475 |
| 18(100/0,2) | 6,50 | 0,071 | 5,720 | - | 2,805 |
| 19(100/0,2) | 4,92 | 0,066 | 4,135 | 6,140 | 1,378 |
| 20(100/0,2) | 5,03 | 0,050 | - | 5,764 | 1,588 |
| 21(100/0,2) | 5,05 | 0,061 | 1,886 | 3,884 | 1,493 |
| 22(100/0,2) | 5,88 | (0,067) | 3,114 | 4,573 | 2,069 |
| 23(100/0,2) | 7,05 | (0,075) | 5,037 | - | - |
| 24(100/0,25) | 4,09 | 0,056 | 2,321 | 3,133 | 1,800 |

Multi-channel recorder used to accurately record $\delta_u$

Table 5.5 (Continued)

(c) Series F3 (Continued)

| Specimen identification | $F_{max}$ (kN) | $\delta_{Fmax}$ (mm) | $\delta_m$ (mm) | $\delta_u$* (mm) | $A_{F,\delta}$ (Nm) |
|---|---|---|---|---|---|
| F3/25(100/0,4) | 3,43 | 0,073 | - | 4,386 | 1,315 |
| 26(100/0,4) | 3,17 | 0,052 | 3,477 | 4,135 | 1,213 |
| 27(100/0,4) | 3,48 | 0,094 | 2,362 | 3,759 | 1,494 |
| 28(100/0,4) | 2,91 | 0,067 | 1,604 | 3,007 | 0,902 |
| 29(100/0,4) | 3,41 | 0,073 | 2,218 | 3,446 | 1,330 |

Note.

1. No result for $\delta_m$, $\delta_u$ or $A_{F,\delta}$ implies full load-deflection curve was not obtained, or recorder was unable to accurately record this value.

2. Results in parentheses indicate that the measured fracture record was considered unreliable, or that one of the calculated results was a statistical outlier.

* Multi-channel recorder used to accurately record $\delta_u$

The representative beams selected were:-

| | | | |
|---|---|---|---|
| SERIES F1 | F1/2 | (500/0,2) | Constant Section |
| (five beams) | F1/4 | (500/0,4) | " " |
| | F1/6 | (300/0,2) | " " |
| | F1/8 | (200/0,4) | " " |
| | F1/14 | (100/0,4) | " " |
| SERIES F2 | F2/1 | (800/0,2) | Variable Section |
| (five beams) | F2/3 | (800/0,4) | " " |
| | F2/7 | (100/0,25) | Constant Section |
| | F2/10 | (100/0,4) | " " |
| | F2/25 | (100/0,5) | " " |
| SERIES F3 | F3/2 | (500/0,2) | Variable Section |
| (nine beams) | F3/4 | (500/0,4) | " " |
| | F3/6 | (300,0,2) | " " |
| | F3/8 | (300/0,25) | " " |
| | F3/11 | (300/0,4) | " " |
| | F3/14 | (200/0,2) | Constant Section |
| | F3/15 | (200/0,4) | " " |
| | F3/19 | (100/0,2) | " " |
| | F3/26 | (100/0,4) | " " |

The load-deflection records were analysed and divided up to give about ten points that were co-ordinated in order to produce the tables in appendix D. Points of rapid change of slope were included, as well as the point representing peak load, i.e. $F_{max}$, $\delta_{Fmax}$. The first point after the origin was chosen to represent the initial point of departure from linearity of the curve, which was important when analysing slow crack growth. It was generally found that the initial portion of the curve was linear allowing a confident determination of the initial slope. However, the choice of the point of departure from linearity was necessarily visual and therefore somewhat subjective, and clearly this technique requires further refinement. In a few cases, for the 100x100x800mm beams of series F2, it was found that the initial portion of the record suffered from extraneous effects such as a slight twist in the beam, and was clearly unrepresentative. However, these records were not discarded since the majority of the record was acceptable, and the initial linear portions were assumed either from the mean values of identical companion specimens or from the theoretical value.

It was considered desirable to compare the shapes of the load-deflection curves on a non-dimensional basis, and therefore the records were processed to produce plots of relative load against relative deflection. This was done by dividing the loads F by the maximum load $F_{max}$, and the deflections $\delta$ by the deflection at maximum load $\delta_{Fmax}$. Typical plots are given later in 5.6.

## 5.4 NOTCH-SENSITIVITY OF FRACTURE BEAMS

A major objective of the present work was to characterise the fracture behaviour of the particular concrete beams as closely as possible. This involved noting the influence of a notch or crack on fracture strength, on deformations in the fracturing cross-section, on beam compliances, and on shapes of load-deflection curves. An important question that required resolution was the degree to which fracture mechanics principles could be applied to the material in the form of notched beam (NB) specimens. The advantage of fracture mechanics, and of linear elastic fracture mechanics (LEFM) in particular, is that it allows a simple estimate of the strength of a member in the presence of stress-raising flaws or notches. One of the basic requirements for the applicability of LEFM to a material is that the notch or crack should exercise a dominant influence on fracture strength; in terms of NB specimens, this implies that the specimen ought to fail such that the net stress at the root of the notch is appreciably less than the modulus of rupture (MR) of the material. Such a material (or specimen) is termed "notch-sensitive". Furthermore, for a notch-sensitive material the net failure stress at the notched cross-section should decrease with increasing notch depth.

The question of notch-sensitivity of cemented materials has been briefly discussed in 2.5.2. There is still controversy as to whether concrete is *actually a notch-sensitive material*, due to conflicting results of different investigators (see figure 2.10). Ziegeldorf et al[94] have shown that notch-sensitivity is a necessary though not sufficient condition for the applicability of LEFM to concrete. This question receives further treatment in chapter 9; however, notch-sensitivity results are presented here as part of the basic fracture test results.

### 5.4.1 CALCULATION OF NET FAILURE STRESS

Considering a notched section with initial notch depth $c_0$ and residual ligament depth $h_0$, the net stress $\sigma_n$ at failure at the root of the notch is:-

$$\sigma_n = \frac{6M_{max}}{bh_0^2} \qquad \text{where } M_{max} \text{ is the moment at failure.} \tag{5.5}$$

The nominal maximum stress ($\sigma$) for the gross section is:-

$$\sigma = \frac{6M_{max}}{bd^2}$$ Therefore, we can write:-

$$\sigma_n = \sigma\left(\frac{d}{h_0}\right)^2 \tag{5.6}$$

where d is the depth of the beam.

In calculating $M_{max}$, applied loads and beam self-weight should be taken into account.

The notch-sensitivity of the beams can be tested by plotting the ratio $\sigma_n/f_r$ *against initial notch depth ratio* $c_0/d$, where $f_r$ is the measured MR of the beams; $\sigma_n/f_r$ is termed the "relative MR". For series F3 beams, MR was measured for virtually every batch of concrete using nominal 100x100x450mm unnotched beams point-loaded at mid-span (see table 5.1(c) for results). For series F1 and F2, only limited MR tests were done on 610mm span beams loaded at the third points. However, reference to figure 5.3 will show that the MR results for series F1, F2 and F3 fell in a consistent band, and a mean line could be drawn through the results parallel to the mean line of Walker and Bloem's results. This mean line could be used together with measured cube strengths to obtain better values of MR for series F1 and F2. The ratios $\sigma_n/f_r$ were calculated taking mean values for $\sigma_n$ and $f_r$ for any particular beam size and initial notch depth ratio. Results are plotted in figure 5.6. A scatter of results has occurred, but clear trends are obvious. It appears that 100mm deep beams are notch-insensitive, the net failure stress actually rising slightly with increasing notch depth. Beams deeper than 100mm show increasing notch-sensitivity with increasing beam depth and increasing notch-depth ratio. Thus, 200mm beams are moderately notch-sensitive, while 300mm, 500mm and 800mm beams are very clearly notch-sensitive. Fracture mechanics principles can therefore be applied to beams of depth greater than 100mm for the present tests. (See chapter 9 for further discussion).

## 5.5 BEAM DEFLECTIONS AT OR NEAR ULTIMATE FRACTURE.

For an accurate assessment of specimen fracture energies, it is necessary to accurately determine two important deflections at or near ultimate fracture:- the deflection at the point when the applied load drops to zero, $\delta_m$, and the deflection at ultimate fracture, $\delta_u$, defined as the point when the crack fully penetrates to the upper face of the beam and final separation occurs. A knowledge of $\delta_m$ is necessary in order to assess work done on the beam by the applied load, while $\delta_u$ is required to assess the contribution of the self-weight to total fracture energy. It will be shown in chapter 9 that incremental fracture energies rise very rapidly during final fracture under the action of self-weight. It is necessary to know $\delta_u$ to properly assess this final fracture energy.

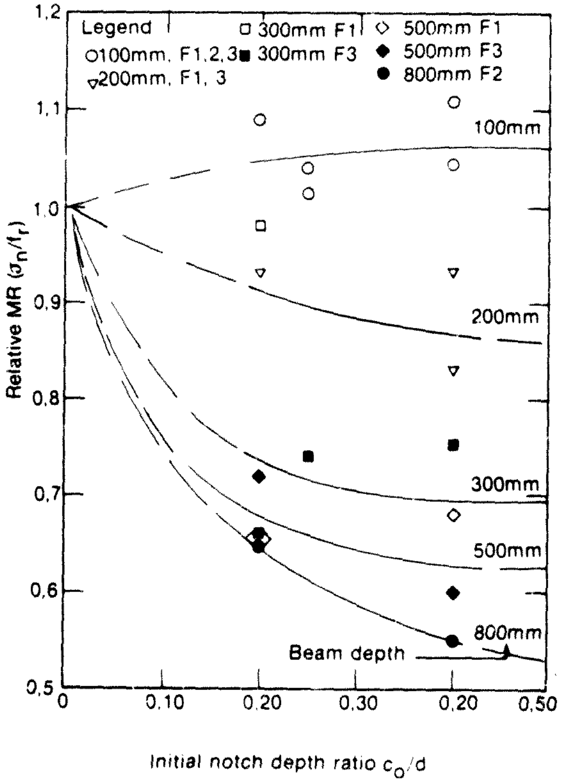


Figure 5.6 Notch-sensitivity of fracture beams (series F1,F2,F3)

Accurate measurement of $\delta_m$ and $\delta_u$ is complicated by the fact that velocities of crack growth and beam deflection increase considerably as final failure is approached. The great majority of the test can be regarded as quasi-static except for that portion near ultimate fracture when transient effects become important. The problem is therefore one of instrumentation. Recording devices must be capable of responding adequately to transient effects and continue to produce a faithful record of deflection at ultimate fracture. The curve obtained from the XY recorder was primarily the one used to analyse the load-deflection record for each beam. However, it was very difficult to accurately determine $\delta_m$ from the XY record, and impossible to determine $\delta_u$. This was because the curve approached the X-axis asymptotically due to the tendency for the rate of beam deflection to increase as ultimate failure was approached. The width of the pen trace also obscured the true point of intersection of the curve with the zero-load axis. Beyond this point of intersection the pen accelerated as ultimate failure was approached, thus rendering $\delta_u$ impossible to measure. The solution was to use an independent strip chart recorder with constant paper speeds, in addition to the XY recorder, as described previously in 4.4.3. Analysis of the records showed that of the two strip-chart recorders, only the multi-channel recorder actually recorded the transient effects of fracture accurately.

Before discussing a typical test record, it is necessary to establish the conditions for which a record is truly representative of beam fracture rather than merely representing the recorder characteristics. Theoretical consideration of the gravitational acceleration of the parts of a fractured beam leads to a second order expression of beam deflection versus time, and hence a record that should appear similar in exaggerated scale to that shown in figure 5.7. Assuming free-fall of the portions of the fractured beam, the velocity of the ends of the beam would quickly become large relative to maximum pen speed of the strip chart. In this case, the record would appear virtually as a straight line at right angles to the direction of chart feed such as line A in the figure. However, there are two factors which render free-fall an impossibility:- firstly, the support condition requires that even after ultimate fracture a small area at the upper face of the beam must remain under slight compression resulting in a few remaining "ligaments" resisting free movement; secondly in order for the beam to deflect vertically downwards it must also spread horizontally outwards at the supports causing frictional resistance which will further restrict free movement. Consequently a more true representation of beam fracture would be a line such as B in figure 5.7.

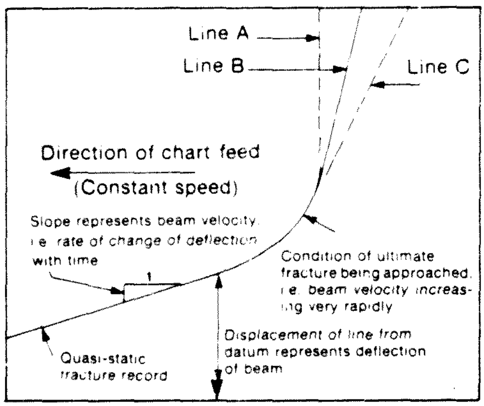


Figure 5.7 Schematic representation of strip-chart record for beam deflection near ultimate fracture

For the recorder faithfully to reproduce line B the pen operating at its free maximum speed should produce a line with a slope steeper than that of the characteristic beam record beyond ultimate fracture, (i.e. a line falling somewhere between lines B and A). Consequently the maximum pen speeds of the recorder must be known, and compared for each record with the actual pen speed after ultimate fracture (as measured by the slope of a line such as B). On this basis, the following argument may be used to decide whether a given record is truly representative of beam fracture:-

1. If the maximum measured pen speed from the record equals the maximum possible pen speed for the recorder, then the charac-

teristics of the pen/recorder are governing the record and the beam velocities will be underestimated.

2. If the maximum measured pen speed from the record is less than the maximum possible pen speed for the recorder, then the record is truly representative of beam behaviour and accurate beam velocities can be measured.

Referring to figure 5.7, the above implies that line B will be accurate if the line representing maximum possible pen speed falls on or between lines B and A, but not accurate if the line lies beyond line B, such as line C. In this case line C will appear as the test record but will merely represent the pen characteristics. The maximum pen speed of a recorder was measured by connecting the recorder to the output from a ± 5mm LVDT, finding the null position of the LVDT, zeroing the trace on the recorder, and then operating the chart drive at maximum speed while at the same time giving the LVDT core a very rapid acceleration. This was done by using a spring-loaded core resting on a support such as the tip of a vertical screwdriver, and then knocking the support away giving virtually instantaneous acceleration to the core. The slope of the trace could be measured, and converted to pen speed using the known chart speed. The following maximum pen speeds were measured:-

Two-Pen Recorder:- 220mm/s (Quoted pen speed from recorder manual was 300mm/s)

Channel 1 of Multi-channel Recorder:- Approximately 6000mm/s

(Note that the above technique was tested on a new strip-chart recorder and the measured pen speed corresponded precisely with the maximum pen speed quoted in the recorder manual, viz 1200mm/s. This give confidence in the use of this simple technique).

As will be shown later, the maximum pen speed of the two-pen recorder was less than that required to faithfully record the beam velocity after final fracture. This was not true of the multi-channel recorder, and only the records from this recorder can be regarded as representative of beam behaviour.

The determination of the deflections $\delta_m$ and $\delta_u$ is best illustrated by reference to an actual test record shown in figure 5.8 (specimen F3/16(200/0,4)). The record shows the final portion of the deflection and load traces on channels 1 and 2 respectively of the multi-channel recorder. Points to note from the record are:-

1. The rate of beam deflection approaching ultimate fracture is roughly constant, and in this case has a value of approximately 0,15mm/s.

2. $\delta_m$ is obtained by determining precisely the point where the load trace drops to zero, and then transferring this position across to the deflection record. The slope of the load trace approaching zero load is very flat due to the small loads involved at this point. However, the F=0 position was accurately determined using a small illuminated microscope (magnification 7x).

3. The rate of beam deflection increases sharply just after the $\delta_m$ position as the beam approaches final fracture under the action of its own self-weight. The deflection trace becomes almost vertical in figure 5.8, and the slope of the straight line portion can be measured with the aid of the microscope. By incorporating chart speed (25mm/s) this slope represents the pen trace speed, in this case 1111mm/s. (The equivalent beam velocity is 69,6mm/s). This figure is less than the maximum pen speed of 6000mm/s. and therefore the trace is representative of beam behaviour.

4. $\delta_u$ is obtained by assuming that the nearly vertical straight line portion of the record represents the downward velocity of the two portions of the beam after final fracture. Consequently the point at which the record becomes a straight line can be taken as the deflection at ultimate fracture, $\delta_u$. This point is found by carefully drawing a fine line to coincide with the final straight line portion of the record, and then using the microscope to determine the point of tangency, i.e. $\delta_u$.

As will be seen later in table 5.6, the falling velocities of the beams were such that recorder pen speeds generally exceeding 500mm/s were required for accurate representation of the fracture record. For this reason the two-pen recorder (maximum pen speed = 220mm/s) was unable to measure transient effects of final fracture accurately.

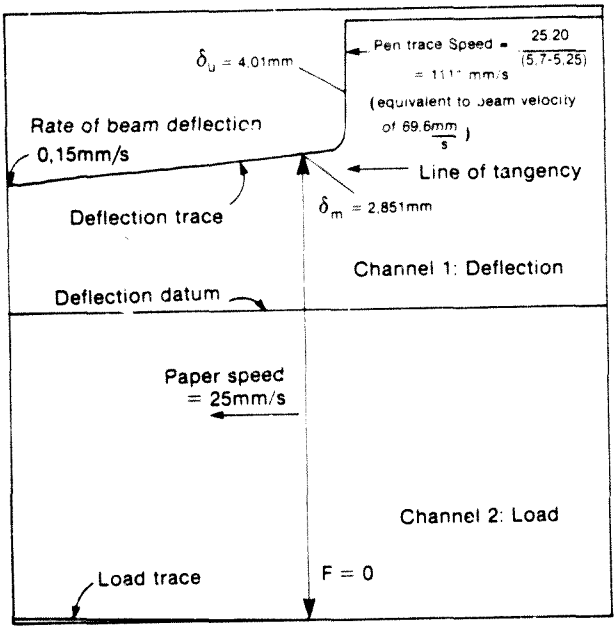


Figure 5.8 Copy of strip-chart record of beam F3/16, showing ultimate fracture

One further point concerning the rate of beam deflections requires mention here. In general, for those beams that were monotonically loaded (mainly series F1 and F2) failure was achieved within thirty to sixty seconds after commencement of loading, but the rate of beam deflection during a test was not necessarily constant. A more rapid rate of deflection usually occurred just after peak load. However, roughly constant deflection rates were achieved before and after peak load, and the values of these rates varied from about 0,02mm/s to about 0,15mm/s. For those beams that were progressively load-cycled to failure (mainly series F3), the total time to failure was increased, being about thirty minutes. However, within any one cycle, the rates of deflection were similar to those quoted above.

### 5.5.1 EFFECT OF FRICTION OF SUPPORT ROLLERS.

For a fracture beam to deflect downwards, particularly at or near the point of ultimate fracture, the two ends of the beam must spread horizontally. This means that restraint of lateral movement will influence fracture test results. A number of different types of lateral movement can occur, depending on the degree of roller fixity and condition of the roller beds:- more or less "free" lateral movement can occur where the support rollers are free to move on bearings, or where they are able to roll laterally on a clean, machined and lubricated bed; lateral movement is restrained or prevented where the rollers are fixed or unable to move due to dirt or rust. The type of roller movement will also dictate whether frictional movement of the specimen ends on the rollers must occur or not. This frictional movement may be either sliding or rolling.

In the present tests, $\delta_u$ was accurately measured for series F3 only, and therefore an assessment of the effects of roller friction must be limited to results of this series. Two types of specimen support were used:- the 100mm deep beams were tested either on the Tinius-Olsen machine which had very limited lateral roller movement since the rollers were supported in concave beds, or on the Amsler machine which had rollers that could move fairly freely on flat machined and oiled base plates; the balance of the beams of series F3 were tested on the Amsler machine, but on occasions the free lateral movement of the rollers was prevented by engaging them with their locating screws. In this way, different types of roller restraint could be examined.

Appreciable roller friction has three major effects that are interrelated:-

1. The fact that additional work must be done to overcome roller friction leads to additional energy being required from the applied load and the beam self-weight.

2. The additional energy is manifested in the test record by an increase in the load and in the values of $\delta_m$ and $\delta_u$.

3. The "dropping" velocity of the beam after final fracture is reduced since roller friction must also be overcome.

Figure 5.9 shows the actual strip chart record of beam F3/9(300/0,25) for which the rollers were fixed during test.

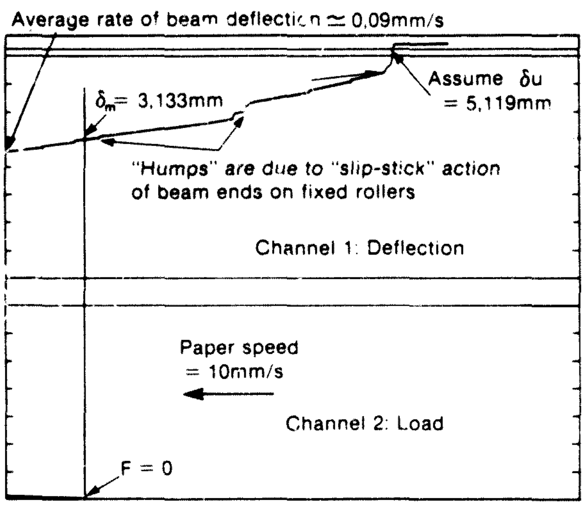


Figure 5.9 Copy of strip-chart record of beam F3/9, showing "slip-stick" friction action

In the case of figure 5.9 beam ends were forced to slide laterally on the rollers, and a clear "slip-stick" action resulted, shown in the figure. The distance along the record between $\delta_m$ and $\delta_u$ is also very much greater than for other beams where the rollers were free (compare figure 5.8) and the values of $\delta_m$ and $\delta_u$ were high relative to other beams (see later table 5.6).

The effects of roller friction on deflections and beam velocities after fracture are shown in table 5.6. The table shows the following trends:-

1. There is a general increase in deflections and a reduction in beam velocities for the fixed roller condition when compared with free rollers.

2. There is a general increase in deflections and decrease in beam velocity with a reduction in beam size. The latter point illustrates the fact that the post-failure velocity will be governed by a residual interaction between the two beam halves, and the larger beams are more able to overcome this restraining interaction by virtue of their self- weight.

3. There is a very large scatter of results indicating that small differances in roller condition or beam friction exercise a large effect on measured values.

The general trends noted above are all consistent with the anticipated effects of appreciable roller friction.

### 5.5.2 THEORETICAL CONSIDERATIONS FOR FIXED ROLLERS.

It is possible theoretically to calculate the energy expended by the beam ends in sliding on fixed rollers. Figure 5.10 shows that for the test geometry, a downward deflection $\delta$ of the centre of a fractured beam results in an amount $\delta$ of horizontal sliding of the

Table 5.6 Analysis of Series F3 to assess effects of support roller condition

| Beam identification | Test machine* & roller condition | $\delta_m$ (mm) | $\delta_u$ (mm) | $\delta_m - \delta_u$ (mm) | Beam velocity after fracture (mm/s) |
|---|---|---|---|---|---|
| F3/1(500/0,2) | A;free | 1,25 | 1,75 | 0,50 | 130,3 |
| F3/2(500/0,2) | A;free | 1,30 | 2,51 | 1,21 | 102,7 |
| F3/3(500/0,4) | A;free | 0,90 | 1,50 | 0,60 | 111,0 |
| F3/4(500/0,4) | A;free | 1,40 | 2,94 | 1,54 | 132,5 |
| F3/6(300/0,[illegible]) | A;fixed | 2,38 | 4,51 | 2,13 | 75,9 |
| F3/8(300/0,25) | A;fixed | 2,72 | 3,82 | 1,10 | 67,7 |
| F3/9(300/0,25) | A;fixed | 3,13 | 5,12 | 1,99 | - |
| F3/10(300/0,4) | A;free | 2,02 | 2,51 | 0,49 | 128,8 |
| F3/11(300/0,4) | A;free | 2,76 | 3,76 | 1,00 | 53,4 |
| F3/12(300/0,4) | A;free | 2,44 | 3,82 | 1,38 | 120,5 |
| F3/13(200/0,2) | A;free | 3,25 | 4,01 | 0,76 | 78,3 |
| F3/14(200/0,2) | A;free | 2,51 | 3,76 | 1,25 | 102,1 |
| F3/15(200/0,4) | A;free | 2,32 | 3,53 | 1,21 | 87,0 |
| F3/16(200/0,4) | A;free | 2,85 | 4,01 | 1,16 | 69,6 |
| F3/17(100/0,2) | T-O;fixed | 3,60 | 5,01 | 1,41 | 84,7 |
| F3/18(100/0,2) | T-O;fixed | 5,72** | - | - | - |
| F3/19(100/0,2) | T-O;fixed | 4,14 | 6,14 | 2,00 | 72,7 |
| F3/20(100/0,2) | T-O;fixed | - | 5,76 | - | 48,6 |
| F3/21(100/0,2) | A;free | 1,89 | 3,88 | 1,99 | 181,6 |
| F3/22(100/0,2) | A;free | 3,11 | 4,57 | 1,46 | 78,3 |
| F3/24(100/0,25) | T-O;fixed | 2,32 | [illegible] | 0,81 | 97,9 |
| F3/25(100/0,4) | T-O;fixed | - | 4,39 | - | 94,9 |
| F3/26(100/0,4) | T-O;fixed | 3,48 | 4,14 | 0,66 | 59,6 |
| F3/27(100/0,4) | A;free | 2,36 | 3,76 | 1,40 | 134,2 |
| F3/28(100/0,4) | A;free | 1,60 | 3,01 | 1,41 | 142,3 |
| F3/29(100/0,4) | A;free | 2,22 | 3,45 | 1,23 | 118,2 |

Notes.

1. *: A = Amsler machine; T-O = Tinius-Ol[illegible]ine.
2. A dash (-) indicates this result [illegible] measured.
3. The results for beams F3/5 and 7, an[illegible] re omitted, in the case of the first two because the mult[illegible]nel recorder was not used, and in the case of the latter because the fracture was deemed unrepresentative (See comments on table 5.5).

** estimate

beam ends on the supports, and this amount will be divided among the supports according to the relative friction operating at each support (shown as equal in the figure).

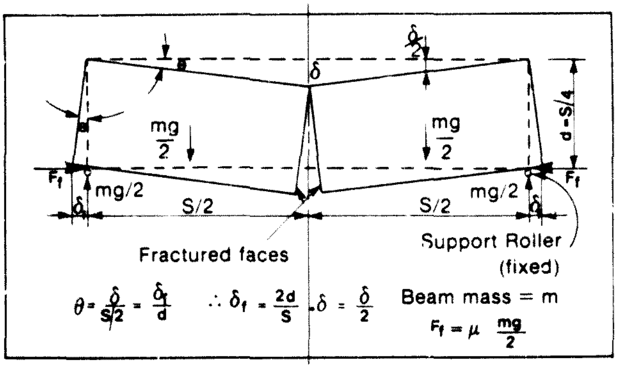


Figure 5.10 Sketch of beam deflections at ultimate fracture

The following energy balance therefore results:-

Since only self-weight acts once the beam deflection equals or exceeds $\delta_m$, the energy provided by the beam in moving through a downward deflection $\delta$ at its centre is:-

$$\text{Self-weight energy} = 2\,\frac{mg}{2}\,\frac{\delta}{2}$$

$$= \frac{mg\,\delta}{2} \qquad (5.7)$$

where mg is the total weight of the beam.

The downward movement is accompanied by outward sliding on the supports, and hence work is done against the horizontal frictional force $F_f$. $F_f$ is governed by the reaction at the supports (mg/2) and by the coefficient of sliding friction, $\mu$, i.e. $F_f = \mu(mg/2)$. Therefore, the total work done against friction is:-

$$\text{Frictional energy} = \mu\,\frac{mg}{2}\left[\frac{\delta}{2} + \frac{\delta}{2}\right]$$

$$= \frac{\mu m g \delta}{2} \qquad (5.8)$$

Comparing the two energies in equations (5.7) and (5.8), the following conclusions can be made:-

1. If $\mu = 1$ the two energies are identical i.e. an energy balance results. Theoretically, the beam should therefore be in stable equilibrium and should move to a new position if induced to do so but then remain static.

2. If $\mu > 1$ frictional energy will outbalance self-weight energy and the beam will tend to "hang-up" without falling.

3. If $\mu < 1$ then additional energy is expended in the form of heat and particle interlock/friction near the top of the two fractured faces during downward movement.

(It is possible that the horizontal sliding movement will be somewhat less than $\delta$ assumed above, since it can be expected that some localised crushing of the mating sections of the fractured faces will occur).

Since measurements of horizontal sliding movement and frictional force were not made, it is not possible to verify the above energy balances from the results directly. However, the following observations on beams with fixed rollers are cited in order to draw rough conclusions:-

1. It is unlikely that the $\mu > 1$ condition was achieved overall, except possibly in the case of F3/20([illegible]). For this fixed roller beam, it was observed from the strip-chart record that the F=0 position (i.e. $\delta_m$ position) lay beyond the $\delta_u$ position, thus apparently indicating that ultimate failure under self-weight never occurred, and a small external load had to be applied to overcome frictional restraint. It is also significant that this beam had the lowest falling velocity of all the 100mm beams of series F3. Further evidence of a possible

$\mu > 1$ condition is the "slip-stick" action described previously with reference to figure 5.9 (beam F3/9). This seems to indicate that, momentarily at least, the $\mu > 1$ condition must have been achieved for this beam.

2. There was a noticeable tendency for the fixed roller beams to "hang-up" before final fracture and take a significantly longer time to move from $\delta_m$ to $\delta_u$. This indicates that $\mu \rightarrow 1$ occurred.

3. If the horizontal sliding movement was significantly less than the vertical movement due to localised crushing of the fractured faces, the possibility of a $\mu > 1$ condition is enhanced, from a consideration of the energy balances given previously.

### 5.5.3 INFLUENCE OF SUPPORT ROLLER FRICTION ON FRACTURE RESULTS.

Certain effects of roller friction have been noted above, in particular the effect on deflections of fracture beams at ultimate failure. Roller friction will also influence fracture results. Since the balance of this thesis is concerned with fracture behaviour of notched concrete beams, it is appropriate to mention briefly the areas where effects of roller friction should be considered.

1. Compliance relationships will be influenced by friction. For any particular deflection, roller friction will tend to increase the external load. Therefore measured compliances will be somewhat underestimated. This is particularly true of the 100mm beams, where the majority of the beams had fixed rollers. However, provided the experimental compliance-crack depth relationship is used consistently, it will be possible to infer crack depths from the relationship.

2. Fracture surface energies (i.e. $\gamma'$ values) will be very significantly affected by friction. This is because friction tends to increase the deflections at ultimate failure, and also to increase the external load required to produce any given increment of crack growth. Therefore a greater area under the load-deflection curve will result when friction is present, leading to a greater $\gamma'$ value. A critical analysis of $\gamma'$ values in chapter 9 will allow a rough estimate of the mean coefficient of friction for the beams.

3. Fracture parameters and fracture zone stresses will tend to be higher when friction acts, due to the somewhat higher loads induced friction. However, this effect will be significant only for intermediate and later loading cycles when beam deflections are increasing and friction is more fully mobilised. This is shown by the fact that for beams of any given depth and initial notch depth, maximum loads for fixed and free roller conditions are essentially the same (see table 5.5).

Note that estimates of microcracked zone size, discussed in chapters 7 and 8, will be unaffected by friction effects, since they are based purely on strain and ultrasonic measurements without direct reference to applied loads.

The overall conclusion is that the effect of roller friction is important, and if true fracture records are to be measured, roller friction should be minimised. These effects will be discussed further in relevant sections of chapters that follow.

## 5.6 CHARACTERISTIC SHAPES OF LOAD-DEFLECTION CURVES

The fracture tests provided load-deflection plots that could be analysed to produce fracture parameters. The curves themselves were characteristic of the geometry and notch depths of the particular beams, and yielded valuable qualitative information on the fracture process. This section considers the characteristic shapes of load-deflection curves and the influencing factors.

Two factors were found to have an important influence on the shapes of the load-deflection curves:- the initial notch depth ratio, and the absolute specimen size.

### 5.6.1 EFFECT OF INITIAL NOTCH DEPTH RATIO.

Figure 5.11, taken from ref. 23, shows that initial notch depth ratio $c_0/d$ has a marked effect on the rate of change of curvature at maximum load, on the absolute deflection at maximum load, and on the post-maximum load behaviour. Unnotched beams generally fractured catastrophically with the load dropping instantaneously to zero. Deeper notching gave a progressively greater degree of post-cracking ductility with a flattening of the load peak and an extension of the tail portion of the curve. The observations from figure 5.11 were borne out in the current tests, as can be seen by reference to figure 5.12. This figure is a comparison of typical relative load-deflection curves for 100mm deep beams. In essence, there does not appear to be a great difference between the curves in figure 5.12, but deeper notching leads to a flattening of the peak and post-peak portions of the curve. For a number of the 100x100x850mm ($c_0/d$ = 0,5) beams, the peak was undefined and a plateau peak region occurred on the test record. Under these circumstances it was difficult to analyse the fracture record for anything more than the effective fracture surface energy. The test records for series F2 also indicated that these specimens had significantly larger scatter of results, particularly for the tail portions of the curves, when compared with the shorter span beams.

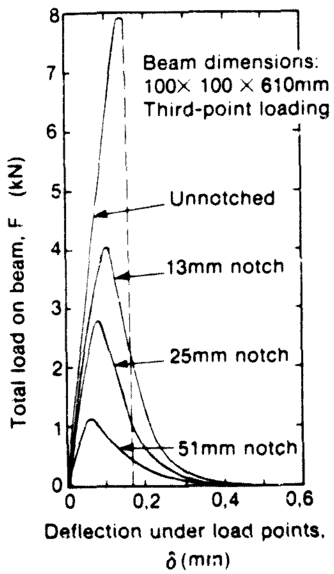


Figure 5.11 Characteristic load-deflection curves for notched and unnotched beams (from ref. 23)

A further effect of notch depth ratio is that shallow notching gives a relatively longer initial linear portion of the load-deflection curve than deep notching where slow crack growth occurs at an earlier stage. This is not always evident from the load-deflection curves, however, since the self-weight has an effect on the load-deflection record particularly of the larger beams, as discussed below.

### 5.6.2 EFFECT OF BEAM DEPTH.

Figure 5.13 shows that, for tl ame $c_0/d$ ratio, the post-peak portion of the curve becomes progressively steeper and the peak more

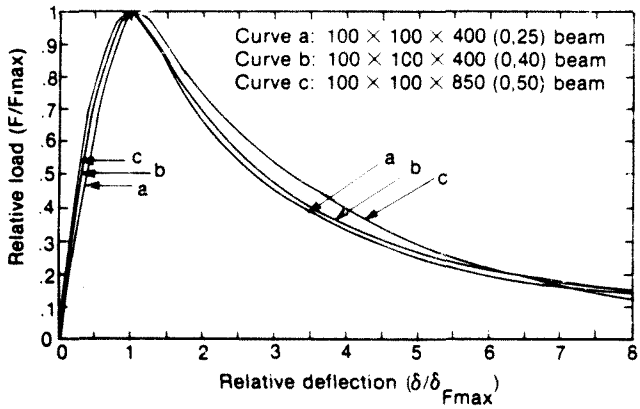


Figure 5.12 Relative load-deflection curves for 100mm deep beams

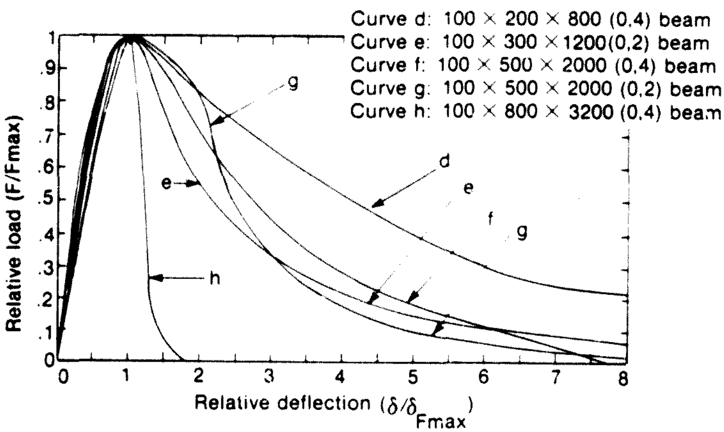


Figure 5.13 Relative load-deflection curves for beams of depth greater than 100mm

pronounced as beam depth increases. The maximum deflection at zero load ($\delta_m$) also generally reduces as beam depth increases, with a dramatic reduction in the case of the 800mm deep variable section beams. (See also table 5.5). Thus, referring to 100mm deep beams, those with a length of 850mm exhibit lower $\delta_m$ values than the 450mm long beams, despite their greater $c_0/d$ ratio. This effect of beam size is primarily that of self- weight, illustrated by the schematic diagram of figure 5.14, an explanation of which follows.

1. Assume points A to G represent the "true" characteristic load-deflection curve for a notched beam. Such a curve would exist if the beam were weightless or if a mechanism existed whereby self-weight could be balanced by an imaginary force equal in magnitude but opposite in direction and acting through the centroids of each half of the beam. The origin of the curve would be at A.

2. Assume that self-weight of magnitude B'B is slowly allowed to act such that an initial linear path AB is followed by the beam. This is equivalent to assuming that the load history of the beam commences at point B, the effect of the self-weight is then removed by the balancing mechanism causing the path BA to be followed, and an external load equal to the self-weight is then re-applied causing the path AB to be followed. At B, therefore, the beam can be regarded as being weightless and acted on by an external load equal to the self-weight in magnitude, sense, and effect.

3. Additional external load is applied to the beam causing the path BDF to be followed , which is the measured load-deflection curve. External work is done on the beam equal to the area BDF, and since the external load drops to zero at point F, it can be assumed that the work is consumed in creating new fracture surfaces. The condition of the beam at point F can be regarded as identical to that at point B discussed above. Point F also represents the maximum deflection at zero load, $\delta_m$.

4. If the imaginary load at F (effectively equal to the self-weight) were slowly reduced while allowing the beam to continue to fracture, the beam would follow the path FG, final fracture occurring at G. Thus the area under FG represents work performed by the imaginary external load and contributes to the fracture energy of the beam.

5. In reality, the full self-weight is applied when the beam is on its supports, and the path AB is initially followed. However, at F the self-weight is acting, although external load (i.e. machine load) is zero. Since the full self-weight must act at all times, it is not possible for the path FG to be followed. Rather, a path similar to FHJ will be followed, such that the areas under FH and FG are equal, and final fracture of the beam under the action of self-weight occurs abruptly at H when self-weight can be regarded as instantaneously reducing to zero at J.

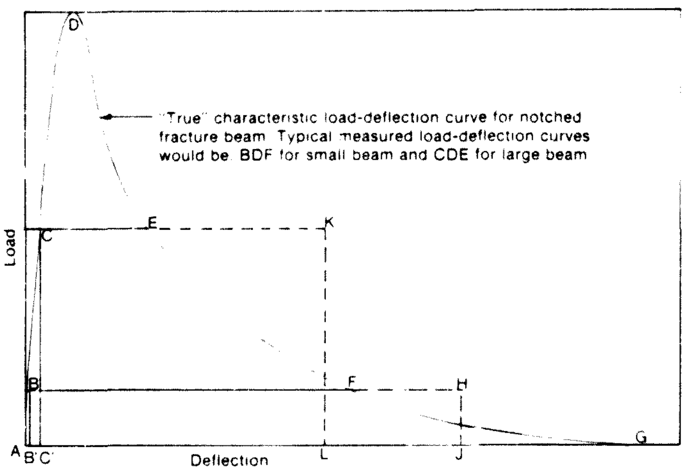


Figure 5.14 Schematic illustration of effect of self-weight on observed load-deflection curve

The argument above can also be applied to the situation where the self-weight of the beam becomes a large proportion C'C of the total load at D. The application of external load causes the load-deflection curve CDE to be measured, and E now represents the point of zero external load with $\delta_m$ being the characteristic measured deflection. Assuming again that self-weight could be slowly reduced from E onwards, the fracture path EFG would be followed. However, the full self-weight acts from E onwards, causing a path EKL to be followed, such that the area under EK is similar to the area under EG.

The consequences of the above illustration can be summarised as follows:-

1. Assuming a characteristic fracture curve exists for beams of a given width but with other fixed geometrical and notch depth ratios, increasing beam size will cause the measured tail portion of the curve to be reduced, i.e. a smaller $\delta_m$ will be measured. In addition, the descending branch of the curve will intersect the zero load axis at a more obtuse angle, a point which is well illustrated in figure 5.13. The reduced $\delta_m$ is not only because of a reduced tail portion but also because of a reduced initial portion of the curve.

2. As the self-weight of a beam increases, so the portion of fracture energy attributable to self-weight becomes increasingly important and cannot be ignored. In the case of very large beams this portion of the fracture energy may well exceed the portion due to external applied load. Furthermore, while it might be acceptable to ignore an area such as ABB' in figure 5.14 without introducing serious error into the fracture energy calculation, it may be unacceptable to ignore an area such as ACC'.

3. Beam size also has a marked effect on the deflection at ultimate fracture ($\delta_u$), represented by points L and J in figure 5.14. This deflection is critical relative to the self-weight component of total fracture energy, but is not easy to measure. The

ratio $\delta_u/\delta_m$ will vary as beam size is varied, and will also depend on support roller conditions. This makes prediction of $\delta_u$ from $\delta_m$ a difficult exercise.

## 5.7 CONCLUDING SUMMARY

This chapter contains basic results from materials control and fracture tests. The following broad conclusions can be drawn:-

1. The materials control tests showed that compressive strength variations occurred due to different curing temperatures, slump values, and possible differences in cement quality. Concerning elastic modulus results in particular, these were processed using an averaging technique for series F1 and F2, and obtained directly from the load-deflection relationships for the fracture beams of series F3. Results for cube strength, modulus of rupture, and elastic modulus were generally consistent with other quoted work.

2. Analysis of fracture loads showed that notch-sensitivity for the concrete tested depended on beam depth. The small 100mm beams were notch-insensitive; beams of 200mm depth or greater were notch-sensitive, the notch-sensitivity increasing as beam depth increased. This implied that fracture mechanics principles cannot be applied directly to the 100mm deep beams.

3. Deflections at or near ultimate fracture must be accurately measured. This implies that adequate recording equipment must be used, with response times capable of recording the transient effects that occur during fracture. Support roller friction was found to influence applied loads and deflections, and results such as beam compliances, effective fracture surface energies, and fracture mechanics parameters, particularly those calculated for intermediate and later loading cycles.

4. Referring to characteristic shapes of load-deflection curves of fracture beams, two factors were found to have an influence:-

   a. Increasing the initial notch depth ratio reduced the initial linear portion of the curve, flattened the peak, and extended the tail portion of the curve. With deep notching ($c_0/d \geq 0{,}5$) it became difficult to define an actual fracture instability condition for the beam.

   b. Increasing the beam size caused a more pronounced peak, a steeper post-peak portion of the curve, and a smaller maximum deflection $\delta_m$. This was a self-weight effect which critically influenced the measured load-deflection relationship relative to the "true" relationship for the beam. The self-weight energy may become extremely large for very large fracture beams, and cannot be neglected.

## PART III CHARACTERISATION OF FRACTURE IN CONCRETE BEAMS:- STUDIES OF CRACK GROWTH AND FRACTURE ZONES

Part III comprises chapters 6 to 8. The main objective of these chapters is to characterise fracture of concrete by a study of the progress of cracking through notched beams, and a study of the development under load of microcracked fracture zones. The experimental techniques used for studying crack growth will be introduced; these were basically compliance relationships linked to visible crack growth, and use of ultrasonic pulses. The importance of assessing slow (sub-critical) crack growth before maximum load will be discussed. The use of strain and ultrasonic pulse velocity measurements for studying the development, size, and nature of fracture zones will be described; relationships between various stress zones in fracture beams will be developed and shown to characterise material fracture behaviour relative to ideal elastic-brittle behaviour. The difference between the behaviour of beams of varying depth will be highlighted.

## NOTE ON FIGURE LEGENDS

The sections which follow discuss experimental results, and the figures contain frequent reference to the fracture beams. A general legend is included immediately below which will apply to the figures. Distinctions are made for various beam depths and beam geometries.

- ● 800mm deep beam, variable section.
- ◇ 500mm deep beam, constant section.
- ◆ 500mm deep beam, variable section.
- □ 300mm deep beam, constant section.
- ■ 300mm deep beam, variable section.
- ▽ 200mm deep beam, constant section.
- ○ 100mm deep beam, constant section.

Figure III.1 General figure legend

# 6 BEAM COMPLIANCE AND SLOW CRACK GROWTH

## 6.1 INTRODUCTION

The compliance of a notched beam is a measure of its deflection response to an applied load for a given load geometry. A beam becomes more compliant as the notch depth increases, and it is this fact that has led researchers to use compliance to indirectly monitor the growth of a crack through a specimen. For plane strain fracture testing of metals, a very limited change in compliance (and hence limited slow crack growth) is allowable for a valid test. However in cemented materials, extensive slow crack growth occurs before fracture instability and very appreciable changes in beam compliance therefore occur. The cemented materials researcher has a very different problem to that facing the fracture metallurgist in accounting for slow crack growth and its effect on fracture parameters; the compliance method represents one way of trying to deal with this problem. The method together with background comment has been covered in chapter 3 (3.4). To summarise, the main problem with use of the compliance technique for cemented materials is the effect of closing stresses across the crack face, causing the compliance of a naturally cracked beam to be less than that of an artificially notched beam for equal flaw lengths. Many researchers have used this method despite its limitations; to ignore slow crack growth in cemented materials is unacceptable, and the main advantage of the compliance method is that it allows an estimate, albeit an imperfect one, of this effect.

## 6.2 CONDITIONS OF FRACTURE INSTABILITY

Slow crack growth and development of a zone of microcracking occurs prior to fracture instability in cemented materials. The point of fracture instability is not always easy to assess since for notched specimens the crack may not grow spontaneously even when the maximum load has been reached. The Griffith criterion for brittle materials (equation (2.2)) implies that at fracture, sufficient elastic strain energy is stored in the specimen to cause the crack to propagate spontaneously through the material, i.e. unstable crack growth occurs. For composite cemented materials which in essence are quasi-ductile rather than brittle, this criterion may be satisfied for unnotched or very shallow-notched specimens. For the majority of specimens tested in the present work, true spontaneous crack propagation leading to ultimate failure did not occur. However, other types of crack propagation occurred, and they may be summarised as:-

1. Stable crack growth. This generally occurred during the load-cycling tests at or just beyond the point of maximum load for each cycle, and was particularly noticeable for the more shallow notched beams (i.e. $c_0/d = 0,2$ or $0,25$). During the period when the load/deflection was held reasonably constant for strain readings to be taken, the deflection (and strains) slowly increased or alternatively the load slowly reduced due to incremental crack extension (and obviously also a degree of creep). (Refer to 4.5.2, and figures 4.6(a) and (b)). It was not possible to detect any advance of the visible crack tip during this process.

2. Unstable crack growth. On occasions, the peak load point during a continuous test or during a load cycle was followed by rapid crack growth leading to a large increase in deflection and reduction in load. In this case, sufficient strain energy was present to cause a substantial advance of the crack tip, although propagation to ultimate failure generally did not occur. Occasionally, slow stable crack growth developed into rapid

unstable crack growth since the slow advance of the crack eventually led to the satisfying of a Griffith-type energy balance.

In view of the above, it is often not easy to mak a precise unambig' us definition of the point of fracture "instability". It is proposed in the present work to regard both of the crack propagation conditions described above as valid instability conditions. In the event that neither of these conditions occurred (as for example in the deeply notched beams), then it is proposed to follow the practice used in testing of metals, viz. that the point of instability of crack extension is the point at which the load-deflection curve reaches a maximum or attains zero slope:-

$$\frac{dF}{d\delta} = 0 \qquad (6.1)$$

It should be noted that the criterion in equation (6.1) very often coincided with the points of stable or unstable crack growth referred to above, particularly for the shallow notched beams. For load-cycled beams, it was possible to produce instability conditions at the peak of most of the earlier cycles during a test, and this allowed the variation of fracture parameters with crack growtl to be studied.

An alternative definition for instability would be the point of departure from linearity of the rising branch of the load-deflection curve. This point is not a condition of crack instability but is rather the initial point at which a significant development of microcracking ahead of the notch begins. It can thus be regarded as the first increment of effective crack growth when energy is being expended on creating damage in the beam.

## 6.3 DERIVATION OF COMPLIANCE - CRACK DEPTH RELATIONSHIPS

The compliance $\lambda$ of a beam is defined as the inverse of the slope of a linear portion of a rising branch of the load-deflection curve, where the load is expressed as the load per unit width of the beam, i.e.:-

$$\lambda = \frac{\delta}{(F/b)_{\text{linear portion}}} \qquad (6.2)$$

Alternatively, the compliance may be defined as the inverse slope of a line joining the origin with some particular point on the load-deflection curve. Both of these definitions are dealt with in the discussion. The relationship between compliance and crack depth can be obtained either by experiment or by theoretical derivation. The experimental method involves measuring the compliance on beams tested with progressively deeper notches. The notch is used to simulate a natural crack, which has limitations as discussed previously. In the theoretical method the conventional relationship is derived from linear-elastic fracture mechanics principles, using the expressions for K (equation (3.2)), G (equation (3.19)), and the relationship between K and G for plane-strain (equation (3.20)). A more general form of derivation is a relationship between $\lambda/\lambda'$ and $c/d$, where $\lambda'$ is the compliance of an unnotched specimen (zero notch depth). This form eliminates the elastic modulus E from the equation, and makes the relationship general for any material, dependent only on Poisson's ratio $\nu$.

Since a notch cannot adequately simulate a natural crack in cemented materials, the conventional compliance-notch depth relationship does not include for the effects of crack-closing stresses. Therefore, for the purposes of this chapter, the theoretical compliance relationship is based on a stress-free crack. However, reference will be made to reloading compliances which effectively include for closing stress effects.

For the present tests, two different beam geometries of either constant or variable section were used. Two theoretical conventional compliance relationships were derived, details of which are given in appendix E. The two curves are shown later in figure 6.2, assuming $\nu$ = 0,15. (Note that although a mean value for $\nu$ of 0,16 was obtained during the materials tests (series F3), a variation of $\nu$ from 0,1 to 0,2 makes very little practical difference he relationship).

## 6.4 METHODS OF OBTAINING COMPLIANCES FROM LOAD-DEFLECTION RECORDS

The conventional method involves taking the compliance as the inverse slope of the line joining any particular point on the curve with the origin. Referring to the load-cycling technique, the point for any cycle is generally taken as the maximum load point, since the visible crack will reach its maximum value at that point. During a test the load was usually rapidly reduced after reaching this point, with little or no additional deflection. As mentioned previously, the conventional method suffers from the influence of a non-linear microcracked zone which is unaccounted for. For this reason, a modified method can be defined, which allows for the influence of the microcracked zone by taking the compliance for each cycle as the inverse slope of the straight line fitted to the re-loading curve at the start of the next cycle. Thus the irrecoverable deformation $\delta_p$ for each cycle is accounted for in the method.

The two methods are illustrated in figure 6.1 (which is based on previous figure 4.6(a), beam F3/15(200/0,4)). For clarity, the bottom loops of the curve for each cycle have been omitted, as well as an initial preloading cycle. The envelope curve has been drawn in to indicate the curve that would have been followed in a continuously increasing deflection test.

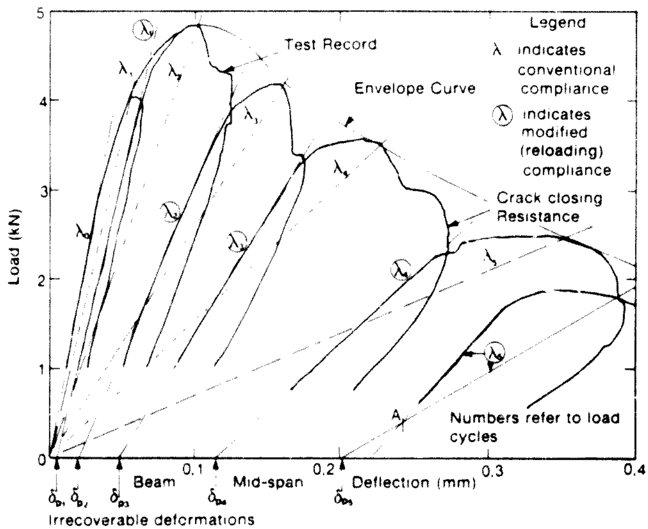


Figure 6.1 Methods of obtaining beam compliances from load-deflection record

Points to note from figure 6.1 are:-

1. There is very little difficulty in defining a modified compliance for each cycle, since the reloading curve has a remarkably linear portion. Towards the end of a test, however, this linear portion was no longer very evident.

2. The conventional peak load compliance is easily defined by the point where the envelope curve intersects the peak of each cycle.

3. The irrecoverable deformations $\delta_p$ are shown on the abscissa axis. They are found by extending the straight line portion of each reloading curve backwards to the axis. It was felt that this was the most logical and consistent method of defining $\delta_p$.

4. The conventional and modified compliances are very similar during the first few cycles, as shown by the similar slopes on the figure. This is due to the irrecoverable deformation initially being relatively small. During later cycles, the two compliances diverge.

5. The unloading curves generally have vertical portions immediately after the peaks of each cycle where load was rapidly "dumped" to prevent rapid crack propagation. These vertical portions of the record have been taken as indicating a positive resistance to crack closing which occurs at the start of the unloading cycle. It is suggested that aggregate particles that have been partially pulled out of the matrix during the loading cycle, as well as delamination and disintegration of crack surfaces, are the main causes of this crack-closing resistance. The resistance is eventually overcome followed by a degree of crack closing. Irrecoverable deformation $\delta_p$ occurs at the end of each cycle, arising from crack-closing resistance. A small degree of resistance to crack opening occurs at the start of a new cycle, but this is less than the closing resistance. Each load cycle results in further aggregate pull-out and crack surface disintegration, giving rise to increasing $\delta_p$ as the test progresses.

6. The reloading curve for cycle 5 shows a change of scale (from the XY recorder,) and the cycle has therefore been defined by slightly extrapolating the envelope curve and re-drawing the reloading slope according to the original scale. The pivot point for the two slopes is marked A in the figure.

7. There is a significant hysteresis loop made by the unloading and reloading curves. This loop is thought to represent primarily damping energy** rather than damage energy, i.e. the energy represented by the area within the loop does not contribute to extension of fracture surfaces in the beam.

8. The fracture energy for each cycle is taken as the slanted area between the straight lines of the reloading curves at the be-

ginning and end of the cycle. This is an idealisation which has also been suggested by Shah and co-workers[41]. The advantage of this definition of fracture energy is that inelastic energies related to the irrecoverable deformations $\delta_p$ are also accounted for. Gurney and Hunt[72] suggest an alternative definition of cyclic fracture energy as the area between the conventional peak load compliance lines and the load-deflection curve (see previous figure 3.12). For cemented materials where inelastic effects are large, however, this method is not suitable.

## 6.5 ELASTIC MODULI FOR SERIES F3 FROM INITIAL COMPLIANCES

It was mentioned in 5.2.3 that elastic moduli for the beams of series F3 were obtained directly from their load-deflection records. The theoretical compliance relationships derived in appendix E show that a direct relationship exists between the unnotched compliance $\lambda'$ and the elastic modulus of the material. There is also a constant numerical ratio between the initial compliance $\lambda_0$ for a beam with any given initial notch depth, and its unnotched compliance, i.e. a ratio $\lambda_0/\lambda'$. These relationships and ratios are given in table 6.1. From the table, elastic modulus can be found from the expression:-

$$E = \frac{k}{\lambda_0} \; \frac{\lambda_0}{\lambda'} \qquad (6.3)$$

where k is 16 or 40,5 for constant or variable section beams respectively, $\lambda_0$ is found from the slope of the linear portion of the initial load cycle, and $(\lambda_0/\lambda')$ is taken from the table for the relevant beam geometry and initial notch depth ratio $c_0/d$.

Table 6.1 Theoretical compliance relationships and ratios

| | Constant section beams | Variable section beams |
|---|---|---|
| Relationship between $\lambda'$ and E | $\lambda' = \frac{16}{E}$ | $\lambda' = \frac{40,495}{E}$ |
| Initial compliance ratios $\lambda_0/\lambda'$ | | |
| $c_0/d = 0,2$ | 1,268 | 1,106 |
| $c_0/d = 0,25$ | 1,443 | 1,175 |
| $c_0/d = 0,4$ | 2,210 | 1,478 |

Elastic moduli for series F3 from (6.3) are given in table 6.2. The variable section beams gave slightly higher E values (mean = 33,5GPa from 12 beams) than the constant section beams (mean = 30,1GPa from 12 beams). Beams with sawn notches have been omitted since the depths of the sawn notches could not be as accurately controlled as the depths of the cast notches. The result for beam F3/27 was statistically tested, found to be an outlier, and therefore excluded. What is of particular note is the consistency of the results, the coefficients of variation being 6,1 per cent and 8,3 per cent for the variable and constant section beams respectively. The results have been condensed by taking mean E values for all beams of a given depth, and have been previously presented in table 5.4.

Table 6.2 Derivation of E values from initial compliances, (Series F3)

| Beam identification F3 | Slope of initial cycle (mm/mm) | Multiplication factor | Initial compliance $\lambda_o$ $(\frac{m^2}{GN})$ | Compliance ratio $\frac{\lambda_o}{\lambda'}$ | E (GPa) |
|---|---|---|---|---|---|
| **Variable section** | | | | | |
| 1(500/0,2) | 0,810 | 1,523 | 1,2336 | 1,106 | 36,31 |
| 2(500/0,2) | 0,440 | 3,046 | 1,3402 | 1,106 | 33,42 |
| 3(500/0,4) | 0,285 | 6,092 | 1,7362 | 1,478 | 34,47 |
| 4(500/0,4) | 0,596 | 3,046 | 1,8154 | 1,478 | 32,97 |
| 5(300/0,2) | 0,885 | 1,523 | 1,3479 | 1,106 | 33,23 |
| 6(300/0,2) | 0,519 | 2,656 | 1,378 | 1,106 | 32,49 |
| 7(300/0,25) | 0,975 | 1,523 | 1,4849 | 1,175 | 32,04 |
| 8(300/0,25) | 0,895 | 1,523 | 1,3631 | 1,175 | 34,91 |
| 9(300/0,25) | 0,455 | 3,046 | 1,3859 | 1,175 | 34,33 |
| 10(300/0,4) | 0,560 | 3,046 | 1,7058 | 1,478 | 35,09 |
| 11(300/0,4) | 0,282 | 6,092 | 1,7179 | 1,478 | 34,84 |
| 12(300/0,4) | 0,605 | 3,046 | 1,8428 | 1,478 | 32,48 |
| **Constant section** | | | | | |
| 13(200/0,2) | 0,383 | 1,523 | 0,5833 | 1,268 | 34,78 |
| 14(200/0,2) | 0,200 | 3,046 | 0,6092 | 1,268 | 33,30 |
| 15(200/0,4) | 0,187 | 6,092 | 1,1392 | 2,210 | 31,04 |
| 16(200/0,4) | 0,188 | 6,092 | 1,1453 | 2,210 | 30,87 |
| 17(100/0,2) | 0,270 | 2,4768 | 0,6687 | 1,268 | 30,34 |
| 18(100/0,2) | 0,142 | 4,9537 | 0,7034 | 1,268 | 28,84 |
| 19(100/0,2) | 0,195 | 3,9616 | 0,7725 | 1,268 | 26,26 |
| 20(100/0,2) | 0,368 | 1,9815 | 0,7292 | 1,268 | 27,82 |
| 21(100/0,2) | (Sawn notch) | | - | - | - |
| 22(100/0,2) | (Sawn notch) | | - | - | - |
| 23(100/0,2) | (Sawn notch) | | - | - | - |
| 24(100/0,25) | 0,350 | 2,4768 | 0,8669 | 1,443 | 26,63 |
| 25(100/0,4) | 0,231 | 4,9537 | 1,1443 | 2,210 | 30,90 |
| 26(100/0,4) | 0,183 | 6,1921 | 1,1332 | 2,210 | 31,20 |
| 27(100/0,4) | 0,145 | 6,092 | 0,8833 | 2,210 | (40,03) (outlier) |
| 28(100/0,4) | 0,196 | 6,092 | 1,1940 | 2,210 | 29,62 |
| 29(100/0,4) | (Sawn notch) | | - | - | - |

Table 6.2 Derivation of E values from initial compliances, (Series F3)

| | Beam identification F3 | Slope of initial cycle (mm/mm) | Multiplication factor | Initial compliance $\lambda_o$ $(\frac{m^2}{GN})$ | Compliance ratio $\frac{\lambda_o}{\lambda'}$ | E (GPa) |
|---|---|---|---|---|---|---|
| Variable section | 1(500/0,2) | 0,810 | 1,523 | 1,2336 | 1,106 | 36,31 |
| | 2(500/0,2) | 0,440 | 3,046 | 1,3402 | 1,106 | 33,42 |
| | 3(500/0,4) | 0,285 | 6,092 | 1,7362 | 1,478 | 34,47 |
| | 4(500/0,4) | 0,596 | 3,046 | 1,8154 | 1,478 | 32,97 |
| | 5(300/0,2) | 0,885 | 1,523 | 1,3479 | 1,106 | 33,23 |
| | 6(300/0,2) | 0,519 | 2,656 | 1,378 | 1,106 | 32,49 |
| | 7(300/0,25) | 0,975 | 1,523 | 1,4849 | 1,175 | 32,04 |
| | 8(300/0,25) | 0,895 | 1,523 | 1,3631 | 1,175 | 34,91 |
| | 9(300/0,25) | 0,455 | 3,046 | 1,3859 | 1,175 | 34,33 |
| | 10(300/0,4) | 0,560 | 3,046 | 1,7058 | 1,478 | 35,09 |
| | 11(300/0,4) | 0,282 | 6,092 | 1,7179 | 1,478 | 34,84 |
| | 12(300/0,4) | 0,605 | 3,046 | 1,8428 | 1,478 | 32,48 |
| Constant section | 13(200/0,2) | 0,383 | 1,523 | 0,5833 | 1,268 | 34,78 |
| | 14(200/0,2) | 0,200 | 3,046 | 0,6092 | 1,268 | 33,30 |
| | 15(200/0,4) | 0,187 | 6,092 | 1,1392 | 2,210 | 31,04 |
| | 16(200/0,4) | 0,188 | 6,092 | 1,1453 | 2,210 | 30,87 |
| | 17(100/0,2) | 0,270 | 2,4768 | 0,6687 | 1,268 | 30,34 |
| | 18(100/0,2) | 0,142 | 4,9537 | 0,7034 | 1,268 | 28,84 |
| | 19(100/0,2) | 0,195 | 3,9616 | 0,7725 | 1,268 | 26,26 |
| | 20(100/0,2) | 0,368 | 1,9815 | 0,7292 | 1,268 | 27,82 |
| | 21(100/0,2). | (Sawn notch) | | - | - | - |
| | 22(100/0,2) | (Sawn notch) | | - | - | - |
| | 23(100/0,2) | (Sawn notch) | | - | - | - |
| | 24(100/0,25) | 0,350 | 2,4768 | 0,8669 | 1,443 | 26,63 |
| | 25(100/0,4) | 0,231 | 4,9537 | 1,1443 | 2,210 | 30,90 |
| | 26(100/0,4) | 0,183 | 6,1921 | 1,1332 | 2,210 | 31,20 |
| | 27(100/0,4) | 0,145 | 6,092 | 0,8833 | 2,210 | (40,03) (outlier) |
| | 28(100/0,4) | 0,196 | 6,092 | 1,1940 | 2,210 | 29,62 |
| | 29(100/0,4) | (Sawn notch) | | - | - | - |

## 6.6 EXPERIMENTAL COMPLIANCE RELATIONSHIPS

The compliance method for assessing slow crack growth is based on measuring the change in compliance between the initial linear portion of the load-deflection curve and the compliance at some other point, and then converting this change into crack growth. To do this, the required compliance is assessed using the theoretical initial compliance, based on the known initial notch-depth ratio ($c_0/d$), to which is added the change in compliance described above. This is a more satisfactory procedure than assessing the required compliance directly from the results, and reduces the spread of values that occur in such testing.

### 6.6.1 INITIAL NOTCH COMPLIANCES

Figure 6.2 shows the theoretical compliance-crack depth relationships for the constant and variable section beams (obtained from data in apppendix E). Initial compliances ($\lambda_0/\lambda'$)for beams of series F1 and F2 are also plotted against initial notch depth ratios ($c_0/d$) to illustrate the typical spread of values. (Series F3 results are omitted since the technique of assessing elastic moduli from the initial compliances would cause these results to fall directly on the theoretical curves). The spread of results increases with increase in the initial notch depth ratio. It was found that, particularly for the 0,5 notch depth ratio beams, the spread of results was very large, and these results are therefore omitted as being unreliable. These comments notwithstanding, the mean values of $\lambda_0/\lambda'$ for all constant section beams of a given $c_0/d$ are close to the theoretical values, indicating that for initial notches where no crack advance has occurred the conventional compliance method is suitable. The inset table in figure 6.2 gives the mean experimental compliance ratios and percentage differences when compared with the theoretical values for the constant section beams. By comparing results for 100mm beams with re s for all

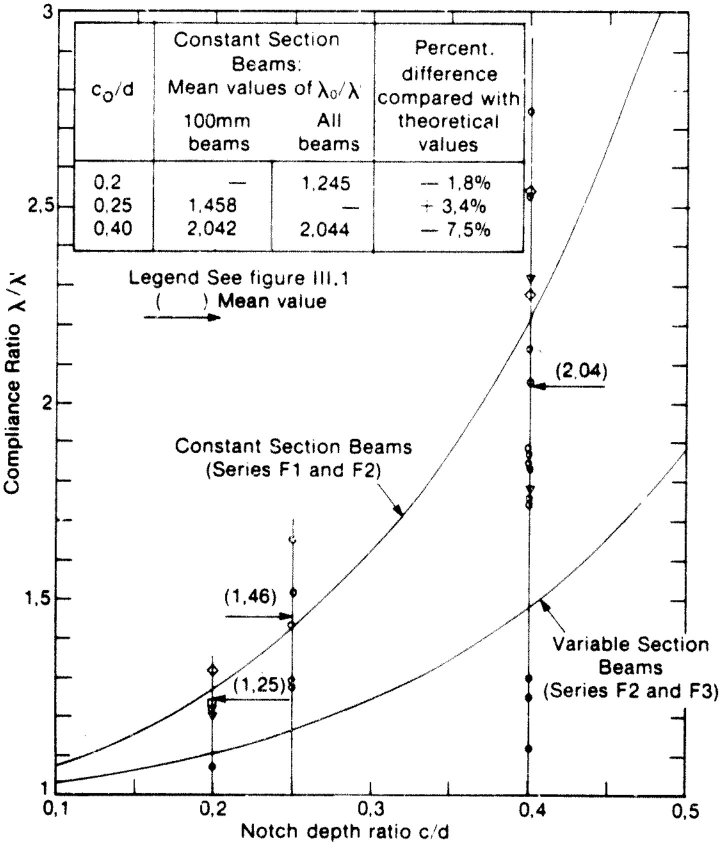


Figure 6.2 Theoretical conventional compliance curves, and comparison with experimental results

beams for $c_0/d$ = 0,4, it appears that there is no practical difference between the results for various sizes. This lends further credence to the method. It was on this basis that the assessment of series F3 elastic moduli from initial compliances was justified.

The results for the four 800mm variable section beams of series F2 are also plotted in figure 6.2. The experimental results fall below the theoretical line, but from an observation of the results for the constant section beams, it appears possible that a similar spread of results could have occurred for the variable section beams and that the theoretical values would be closely matched by the experimental values, for initial compliances.

The different forms of the compliance curves for the constant and variable section beams are noteworthy, since it is the profile of the variable section beams that has caused this effect. These beams are in fact more compliant than the constant section beams due to the tapered section, but for a given increment of crack growth the change in compliance ratio for the variable section beams is less than for the constant section beams. This implies that the determination of a critical crack depth from compliance measurements is more sensitive for the variable section as compared with the constant section beams. This is generally true for c/d ratios less than about 0,4; for c/d greater than 0,5 the sensitivity of crack depth with respect to compliance decreases. On the other hand at large values of c/d, a small change in crack depth results in a large change in compliance, and in this sense the sensitivity of both types of beam increases as c/d increases.

### 6.6.2 COMPLIANCE RELATIONSHIPS FOR SERIES F3

Measurement of visible crack depths for series F3 allowed experimental compliance - crack depth relationships to be obtained. Initial notch compliances were used to assess elastic moduli, and therefore these initial experimental points fell directly on the theoretical curves. Compliances of subsequent cycles were then measured in the conventional way, and expressed as ratios of the theoretical unnotched compliance $\lambda'$. These ratios could be plotted against the visible crack depth ratio, and compared with the theoretical curves. The results are shown in figures 6.3(a) and (b). Note the following from the figures:-

1. A fairly large scatter of results has occurred, although this is accentuated by plotting results for all beams of a given type on one diagram. Generally the experimental points fall above the theoretical curve, and a rough experimental curve can be drawn through the points.

2. Points which are circled represent results for the maximum load cycle, and it is evident that a significant change in compliance has occurred from the initial value. This is due to crack extension from the notch root and development of a microcracked zone ahead of the main crack tip.

3. The fact that the experimental points lie above the theoretical curve implies that beam compliance related to visible crack depth is greater than that predicted from the conventional relation. This is consistent with the development of a microcracked zone which would render the beam more compliant. Alternatively, the measured compliance would lead to a stress-free crack depth which would be longer than the visible crack depth, on the basis of conventional compliance.

The presence of a microcracked zone ahead of the main crack has been mentioned in chapter 3 (3.5). The compliance curves help to shed light on the problem of estimating the size of such a zone. The argument may be presented as follows:-

1. Using the conventional compliance curve, crack depths can be inferred from measured compliances. These crack depths might be termed "apparent" crack depths in the sense that they refer to stress-free cracks, which of course do not exist in real--

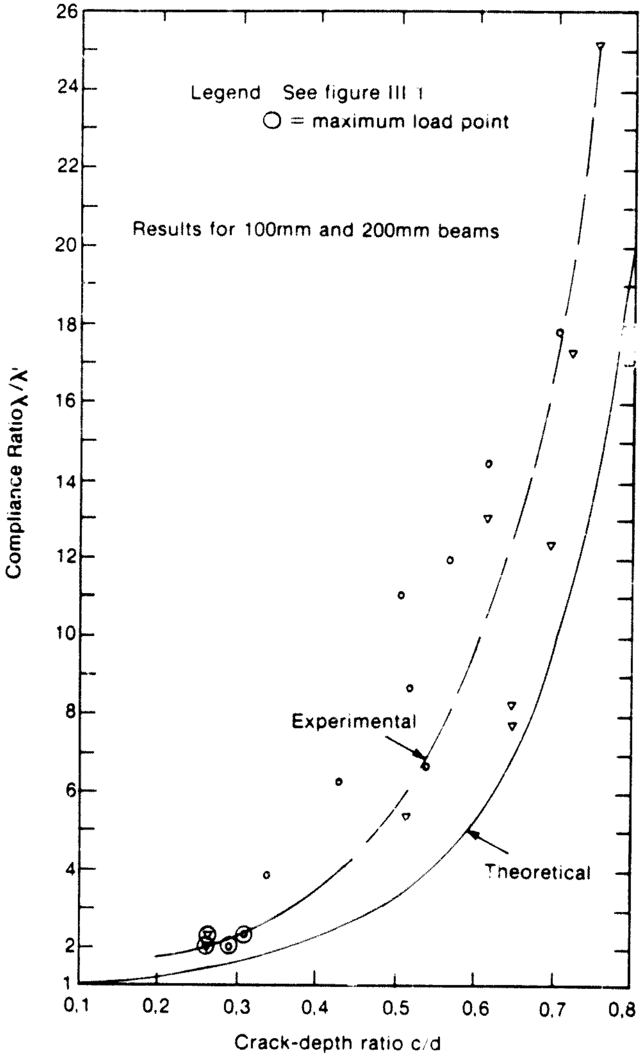


Figure 6.3(a) Experimental compliance relationship for constant section beams (series F3)

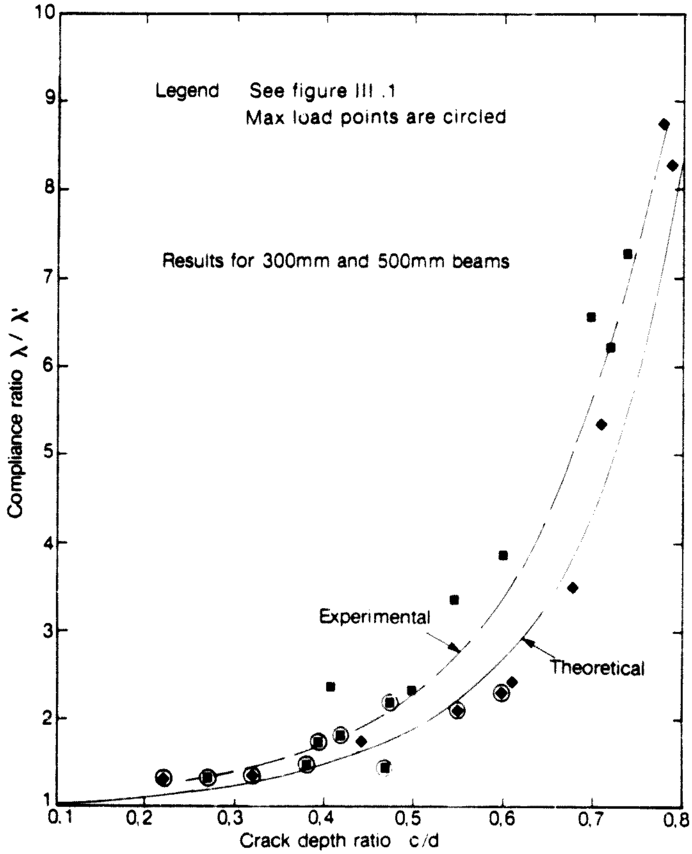


Figure 6.3(b) Experimental compliance relationship for variable section beams (series F3)

2. The visible crack depth $c_{vis}$ corresponding to any particular compliance will be shorter than the "apparent" crack depth $c_{app}$. This is shown schematically in figure 6.4. Also shown in the figure is a microcracked zone ahead of the visible crack tip.

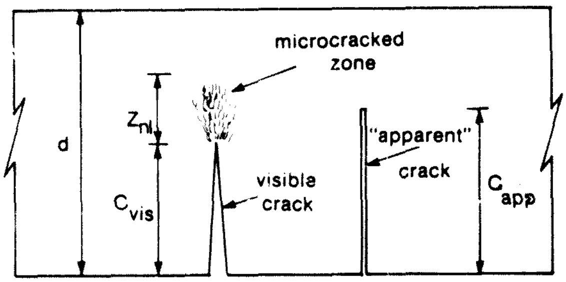


Figure 6.4 Representation of various types of crack in a fracture beam

3. In order for the compliance of a beam containing the stress-free crack plus non-linear zone to equal that of a beam containing an "apparent" stress-free crack only, the length of the non-linear zone ($z_{nl}$) must exceed the difference between $c_{app}$ and $c_{vis}$. i.e.

$$z_{nl} > c_{app} - c_{vis} \tag{6.4}$$

This is because the non-linear zone exerts a stiffening effect on the beam due to the closing stresses operating across the zone, and must therefore extend above $c_{app}$ to allow additional softening to occur.

Hence the difference in the abscissa value between an experimental compliance point and the theoretical compliance curve gives a lower bound to the depth of the non-linear zone. However, as will be shown below, the irrecoverable deformation $\delta_p$ has a dominant influence on measured compliance making this lower bound no more than a crude first estimate of non-linear zone size.

2. The visible crack depth $c_{vis}$ corresponding to any particular compliance will be shorter than the "apparent" crack depth $c_{app}$. This is shown schematically in figure 6.4. Also shown in the figure is a microcracked zone ahead of the visible crack tip.

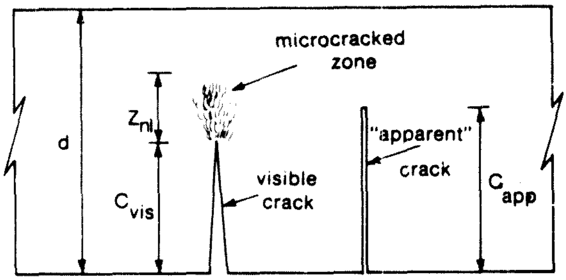


Figure 6.4 Representation of various types of crack in a fracture beam

3. In order for the compliance of a beam containing the stress-free crack plus non-linear zone to equal that of a beam containing an "apparent" stress-free crack only, the length of the non-linear zone ($z_{nl}$) must exceed the difference between $c_{app}$ and $c_{vis}$. i.e.

$$z_{nl} > c_{app} - c_{vis} \tag{6.4}$$

This is because the non-linear zone exerts a stiffening effect on the beam due to the closing stresses operating across the zone, and must therefore extend above $c_{app}$ to allow additional softening to occur.

Hence the difference in the abscissa value between an experimental compliance point and the theoretical compliance curve gives a lower bound to the depth of the non-linear zone. However, as will be shown below, the irrecoverable deformation $\delta_p$ has a dominant influence on measured compliance making this lower bound no more than a crude first estimate of non-linear zone size.

### 6.6.3 EFFECT OF BEAM DEPTH ON EXPERIMENTAL COMPLIANCES AND IRRECOVERABLE DEFORMATIONS

The trend of figures 6.3(a) and (b) seem to indicate that the experimental compliance relationship approximated more closely to the theoretical curves as the beam depth increased. To test this, the compliance relationships were reduced to a common base and expressed in terms of relative compliance values. This allowed a direct comparison between the results of the constant and variable section beams, and between beams of different depths. The results were reduced as follows:-

#### VARIABLE SECTION BEAMS

1. The theoretical compliance curve for variable section beams was adopted as the base curve.

2. Compliance results ($\lambda/\lambda'$) for variable section beams (500mm and 300mm deep) were converted into relative values by dividing all results by the theoretical $\lambda/\lambda'$ value at $c/d = 0,8$ (i.e. 8,219). The theoretical compliance curve was similarly reduced so that an ordinate value of 1,0 was obtained at $c/d = 0,8$.

3. The experimental results were then plotted on separate curves for each set of beams of a given depth. These results are shown in figures 6.5(c) and (d).

#### CONSTANT SECTION BEAMS

1. The compliance curve for the constant section beams had a different form to the variable section curve. Therefore it was necessary to first "conform" the constant section curve to the variable section curve, by taking the ratio, at each particular

c/d value, of $\lambda/\lambda'$ (variable section) to $\lambda/\lambda'$ (constant section) where the $\lambda/\lambda'$ values were taken from the theoretical compliance relation. To simplify matters, a curve of the above ratio versus c/d was plotted and used to assess values of the ratio for the c/d values obtained in the experiments.

2. The experimental compliance values ($\lambda/\lambda'$) for the constant section beams were "conformed" by multiplying them by the relevant ratio of variable to constant section compliance found as in 1. above. These "conformed" values were then converted into relative values in exactly the same way as for the variable section beams, i.e. by dividing them by the theoretical $\lambda/\lambda'$ value at c/d = 0,8 for variable section beams.

3. An example of reduction of results for a variable and constant section beam is shown in table 6.3. The compliance ratios in column 5 were obtained directly from the test record; the "conform" factor in column 6 is the factor required to conform the constant section compliances to equivalent variable section compliances; the relative $\lambda/\lambda'$ value in column 7 is obtained as the product of the values in columns 5 and 6 divided by 8,219. All the conformed and reduced results were then plotted on separate curves for each set of beams of a given depth; see figures 6.5(a) and (b).

Note the following from figure 6.5:-

1. Initial notch depth ratio has no effect on the experimental compliance relation. This is shown by the points for the various initial notch depths forming a consistent and uniform trend.

2. A clear improvement in experimental relationship relative to the theoretical curve occurs as beam depth increases. The experimental curve for the 500mm beams is virtually coincident with the theoretical curve. There is also a slight improvement when going from the 200mm beam to the 300mm beam curves. The experimental scatter reduces as beam depth increases, this is

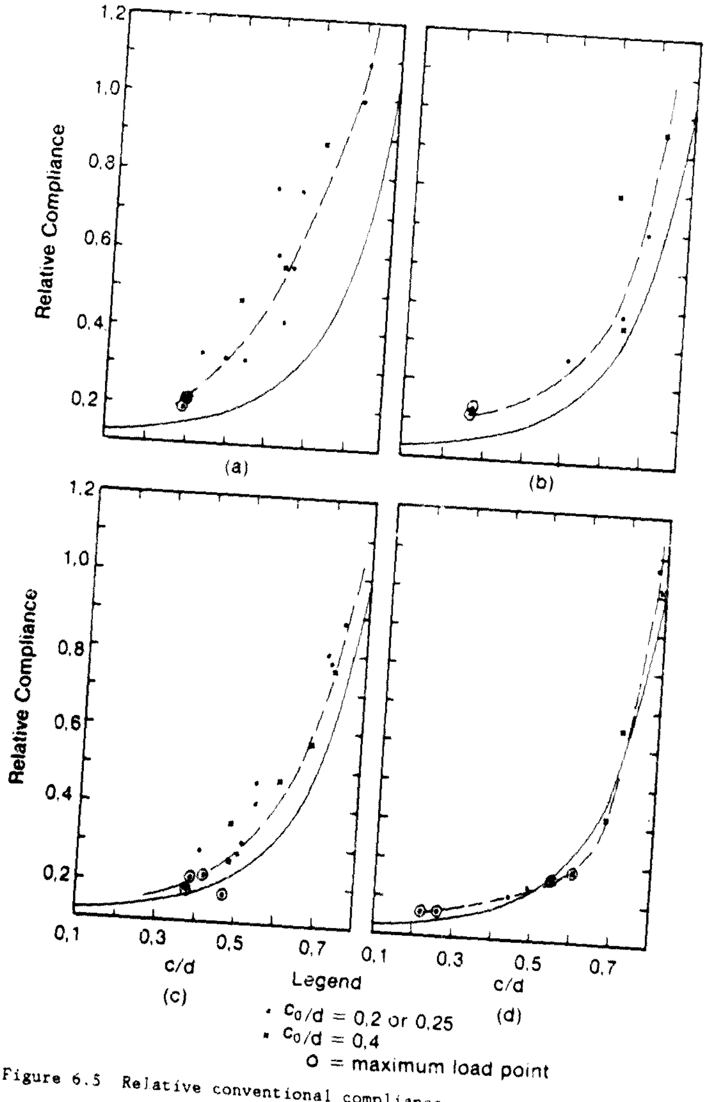


Figure 6.5 Relative conventional compliance curves for beam depths of (a) 100mm (b) 200mm (c) 300mm (d) 500mm (series F3)

Table 6.3 Example of reduction of compliance results for relative compliance curves

| Beam identification | Cycle No. | Visible crack depth c (mm) | $\frac{c}{d}$ | Compliance ratio $\lambda/\lambda'$ | "Conform" factor | Relative $\lambda/\lambda'$ |
|---|---|---|---|---|---|---|
| F3/8 | 0 | 75 | 0,25 | 1,18 | 1,0 | 0,143 |
| (300/0,25) | 3* | 116 | 0,39 | 1,76 | 1,0 | 0,21 |
| Variable | 4 | 149 | 0,50 | 2,31 | 1,0 | 0,28 |
| section | 5 | 161 | 0,54 | 3,36 | 1,0 | 0,41 |
| | 6 | 209 | 0,70 | 6,59 | 1,0 | 0,80 |
| F3/14 | 0 | 40 | 0,20 | 1,27 | 0,88 | 0,135 |
| (200/0,2) | 3* | 53 | 0,27 | 2,21 | 0,81 | 0,22 |
| Constant | 4 | 103 | 0,52 | 5,26 | 0,57 | 0,36 |
| section | 5 | 130 | 0,65 | 8,25 | 0,48 | 0,48 |
| | 6 | 140 | 0,70 | 12,28 | 0,46 | 0,69 |

Note. 1. *refers to max. load cycle.

2. It was difficult to observe visible crack growth during cycles 1 and 2 which were before max. load.

3. Cycle 0 represents the initial compliance value.

despite the fact that fewer experimental points were available for the 200mm and 500mm beams than for the 100mm and 300mm beams. The fact that a crossover occurs between the experimental and theoretical curves in figure 6.5(d) might be due simply to the limited number of experimental results. Alternatively, it might be due to effects of crack-closing stresses in the fracture zone, since reloading compliance curves plotted later show the same trend. (See figure 6.8 later)

The implication of the above is that more serious errors in estimating crack depth will be induced for smaller beams than for larger beams. Reasons for the clear trend shift in figure 6.5 include the following:-

1. Considering firstly experimental accuracy, it is easier to estimate a crack depth visually in large beams than small beams. Also, a given absolute error in crack depth will have a far smaller effect on the compliance relation for large beams than small ones.

2. Secondly, and more importantly, the irrecoverable deformations $\delta_p$ and reloading compliances are critical in influencing experimental compliance relations. Consider figure 6.6, which shows the results from series F3 in terms of $\delta_p$ values plotted against visible crack depth ratios. A large scatter of results occurs; this is to be expected since the nature of the material is that of discrete aggregate particles randomly embedded in a matrix, and the crack-closing resistance offered by the random particles will differ greatly from specimen to specimen. (It may be noted that the effect of initial $c_0/d$ on $\delta_p$ was checked on a preliminary plot, and found to be negligible; therefore all results are plotted on a single graph in figure 6.6). The trend is that the larger beams have larger $\delta_p$ values; however the ratio of $\delta_p$ between, say, the 500mm and 100mm beams is at most about 2, and reduces for smaller c/d. In fact up to c/d = 0,4, there is very little difference between the results. Considering the rotations or relative deflections (i.e. $\delta_p$ di-

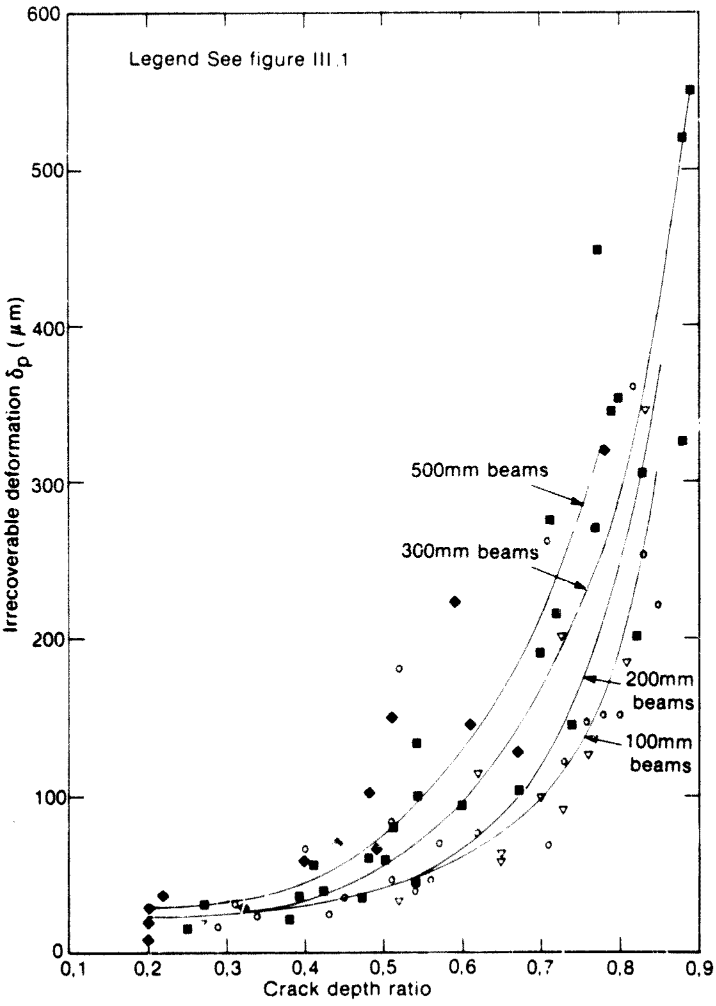


Figure 6.6 Irrecoverable deformations in fracture beams

vided by beam span) of the small and large beams, we can write the following:-

Relative deflection of 100mm beams $= \left(\frac{\delta_p}{S}\right)_{100}$

Relative deflection of 500mm beams $= \left(\frac{\delta_p}{S}\right)_{500}$

Ratio of relative deflections $= \left(\frac{\delta_p}{S}\right)_{100} \div \left(\frac{\delta_p}{S}\right)_{500}$

$$= \frac{(\delta_p)_{100}}{(\delta p)_{500}} \times \frac{(S)_{500}}{(S)_{100}}$$

$$= \tfrac{1}{2} \times 5$$

$$= 2{,}5$$

Since the beam rotations result from the rotation of the crack faces relative to each other, the small beams will experience considerably greater crack face rotations for a given c/d than the larger beams. This is shown schematically in figure 6.7, and results in considerably greater aggregate pull-out and crack surface disintegration for the smaller beams. Thus it might be expected that the influence of closing stresses in the microcracked zone would be very much less in small beams than large beams where less separation of crack faces occurs for a given c/d. This is a tentative conclusion concerning the magnitude of the average stresses in the microcracked zone that will receive further attention in chapter 9.

Not only conventional but also modified compliances (i.e. reloading compliances) will be greater in small beams when compared with large beams. This is borne out in figures 6.8(a) to (d) which show reloading compliances plotted against visible crack depth ratio c/d. There is a clear change in trend of the curves as beam depth increases. The 100mm curve is displaced vertically above the theoretical curve, but retains the same basic shape. The same comment applies to the 200mm beams. The 300mm and 500mm beams have experimental curves that are flatter than the theoretical, with a crossover that occurs at smaller crack depths as beam depth increases. It is postulated that these different curves are due primarily to the nature of stresses in the microcracked zone. Lower stresses exist in smaller beams due to greater relative rotations, and this zone has limited influence on the basic shape of the curve, merely causing it to be displaced upwards. In larger beams, considerable stresses exist in this zone, and the effect is to cause the beam to "stiffen" as crack depth increases. Comparison of figure 6.8 with 6.5 shows that conventional compliance does not monitor the influence of the microcracked zone as well as reloading compliance. The above postulate receives further attention in later chapters.

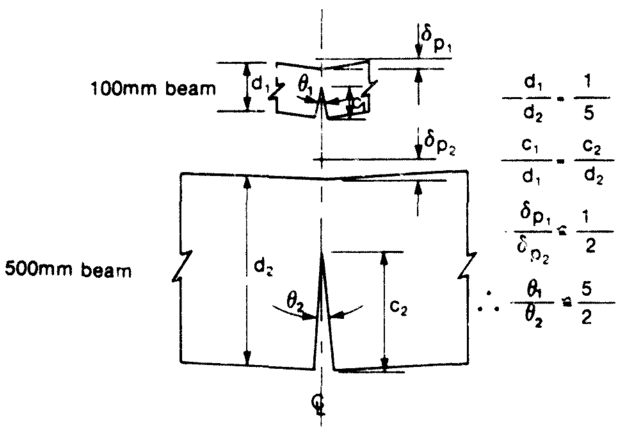


Figure 6.7 Beam rotations due to irrecoverable deformation $\delta_p$

One further point from figures 6.5 and 6.8 is the rapid increase in compliance from the initial notch compliance, even before visible crack growth has occurred. This is due to the development of a microcracked zone ahead of the notch, which increases the beam compliance. As crack extension occurs, the influence of this zone will gradually diminish as the zone itself reduces in size.

imental curves that are flatter than the theoretical, with a crossover that occurs at smaller crack depths as beam depth increases. It is postulated that these different curves are due primarily to the nature of stresses in the microcracked zone. Lower stresses exist in smaller beams due to greater relative rotations, and this zone has limited influence on the basic shape of the curve, merely causing it to be displaced upwards. In larger beams, considerable stresses exist in this zone, and the effect is to cause the beam to "stiffen" as crack depth increases. Comparison of figure 6.8 with 6.5 shows that conventional compliance does not monitor the influence of the microcracked zone as well as reloading compliance. The above postulate receives further attention in later chapters.

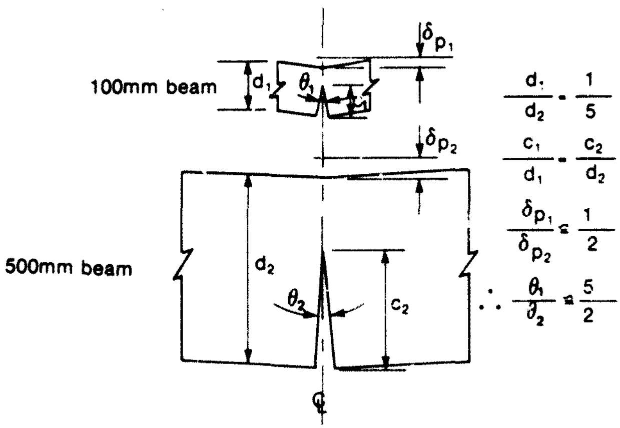


Figure 6.7 Beam rotations due to irrecoverable deformation $\delta_p$

One further point from figures 6.5 and 6.8 is the rapid increase in compliance from the initial notch compliance, even before visible crack growth has occurred. This is due to the development of a microcracked zone ahead of the notch, which increases the beam compliance. As crack extension occurs, the influence of this zone will gradually diminish as the zone itself reduces in size.

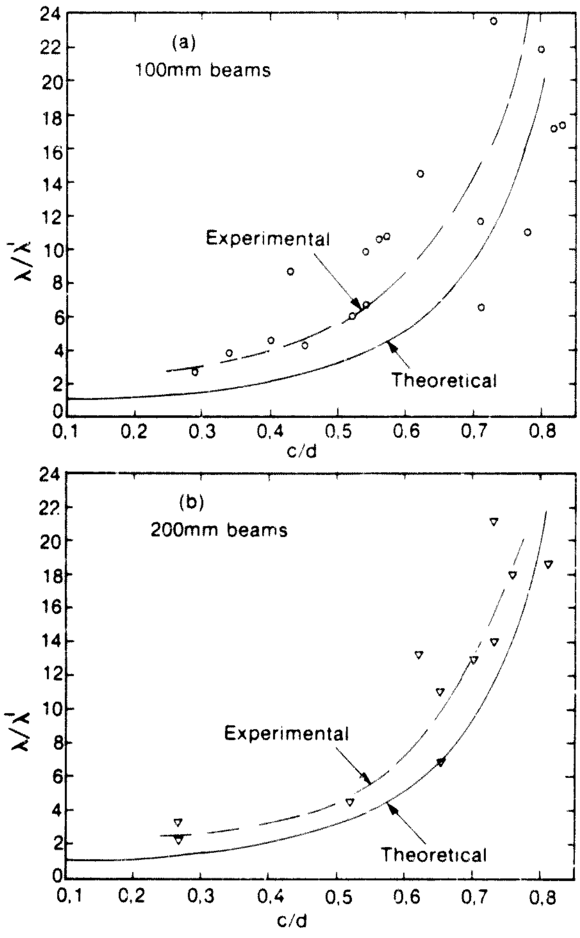


Figure 6.8 Reloading compliance curves for beam depths of (a) 100mm (b) 200mm (series F3)

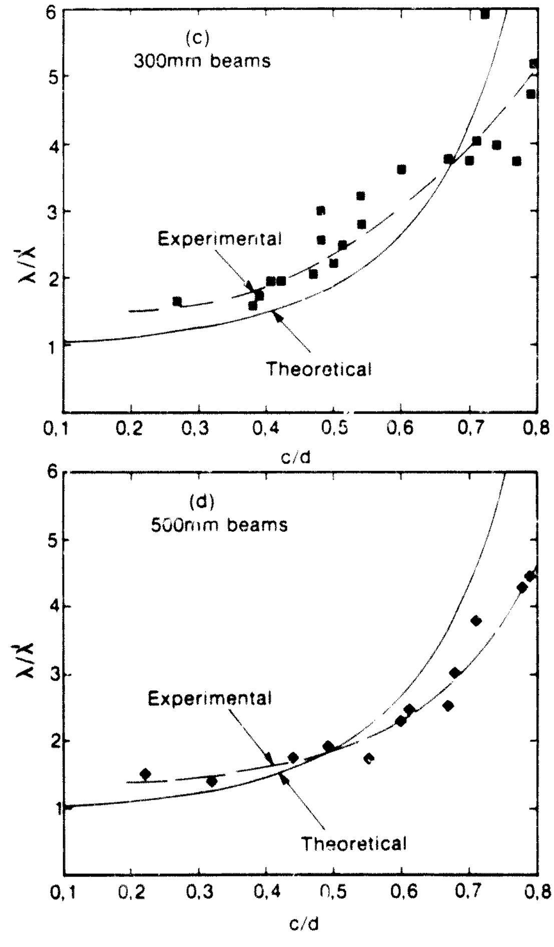


Figure 6.8(continued) Reloading compliance curves for beam depths of (c) 300mm (d) 500mm (series F3)

It should be noted that some inaccuracy in compliance measurements has been introduced by the fact that firstly the load was not always removed immediately the peak load for the cycle was achieved (i.e. some additional crack growth could have occurred before unloading) and secondly $\delta_p$ was influenced by creep during the time taken to record strains. Both of these effects can be noted in figure 6.1. The effect of these inaccuracies is to cause conventional compliances to be slightly underestimated, and to somewhat increase the area under the load-deflection curve. The magnitude of the inaccuracies were considered to be small relative to the scatter of results.

## 6.7 SLOW CRACK GROWTH IN FRACTURE BEAMS

The compliance method outlined previously may be used to assess slow crack growth during a test. However, in cemented materials the problem exists of defining exactly what is meant by crack growth. This might be visible crack growth, or development of a microcracked zone, or increase in effective crack depth (where effective crack depth is the sum of stress-free crack depth and the depth of the microcracked zone). At this point, we do not yet have a reasonable estimate of the depth of the microcracked zone, and therefore it is proposed to use the concept of "apparent" crack depth introduced in 6.6.2. This is the crack depth inferred from the conventional compliance relationship using measured compliance changes. This apparent crack depth will generally be longer than the visible crack depth but shorter than the effective crack depth, as was shown in figure 6.4. Accepting this limitation, it is nevertheless true that the apparent crack depth will give some physical measure of the extent of crack growth during a test, and will allow us to compare the behaviour of different beam sizes.

In this section, the apparent crack growth occurring at maximum load will be examined, since this point is often used to assess fracture parameters. Many investigators have assumed that no crack growth